The Observability of Abundance Ratio Effects in Dynamically Hot Stellar Systems

Jedidiah Serven, Guy Worthey

Program in Astronomy, Washington State University, Pullman, WA 99164-2814

gworthey@wsu.edu

Michael M. Briley[1]

Department of Physics and Astronomy, University of Wisconsin Oshkosh, 800 Algoma Boulevard, Oshkosh, WI 54901

mike@maxwell.phys.uwosh.edu

Department of Physics and Astronomy, University of Wisconsin Oshkosh, 800 Algoma Boulevard, Oshkosh, WI 54901

mike@maxwell.phys.uwosh.edu

ABSTRACT

Using synthetic spectra, we construct a simple model of an elliptical galaxy with a velocity dispersion $\sigma = 200$ km s^{-1}. Absorption feature indices are defined that are sensitive to the abundances of C, N, O, Na, Mg, Al, Si, S, K, Ca, Sc, Ti, V, Cr, Mn, Fe, Co, Ni, Cu, Zn, Sr, Ba, and Eu as a first step in determining the abundances of these elements in stellar populations such as elliptical galaxies for which integrated spectra are available. Using these indices and assuming a photon statistical error such that S/N = 100 around 5000Å, the feasibility of measuring individual elements in real galaxies is assessed. Of the elements studied, only S, K, Cu, Zn, and Eu appear to be difficult to determine. The rest appear to be measurable with high quality data and models. The effects of abundance changes on Lick/IDS indices, Rose indices, and $BRVI$ colors are also tabulated.

Subject headings: galaxies: abundances — galaxies: elliptical and lenticular, cD — galaxies: chemical evolution — stars: abundances — stars: atmospheres

[1]On assignment to the National Science Foundation, 4201 Wilson Boulevard, Arlington, VA 22230. Any opinions, findings, conclusions and recommendations expressed in this material are those of the author and do not necessarily reflect the views of the National Science Foundation.

1. Introduction

A stellar system can be studied by taking a spectrum of it, not star by star, but whatever stars are present in the aperture of the spectrograph. In the absence of complications like nebular emission, dust screening, or the presence of unexpected stellar populations, the spectrum is an integrated, but purely stellar, fingerprint of the ages and abundances of stars that are present. Dynamically hot stellar systems like elliptical galaxies, S0 galaxies, star clusters, and the bulges of spiral galaxies tend to be relatively free of gas and dust compared to disk galaxies (Knapp 1999; Oosterloo et al. 2002). The mixture of stellar populations in these systems is therefore likely to contain only small quantities of very young stars, nebular gas, or dust, making them amenable to analysis via stellar population models.

Current models (Worthey 1994; Bruzual & Charlot 2003; Maraston 2005) universally indicate that two main parameters control the basically one-dimensional continuum in color or spectral feature strength of simple integrated-light systems: age and abundance. The "3/2 rule" of Worthey (1994) states that if an age change is opposed by an abundance change such that d log(age) $= -\frac{3}{2}d$ log(abundance) then very little spectral change will occur: the colors, surface brightness fluctuation magnitudes, and absorption feature strengths will remain essentially the same. Worthey (1994) pointed out that this presents an opportunity to discover abundance ratio variations (non lockstep abundance changes for individual elements) *without* having to know the absolute age or metallicity to very high precision if features could be found in the spectrum that were sensitive to such non lockstep behavior.

Worthey et al. (1992) presented models and observations that seemed to indicate that elemental abundances could decouple in real galaxies by plotting Mg and Fe absorption feature indices for models and elliptical galaxies. The models were for different single-burst ages and abundances and fell along a one-dimensional, highly degenerate trajectory where any reasonable change of age or abundance merely moved an object back and forth along this line. The galaxies, however, drifted off the model sequence such that larger galaxies had very strong Mg feature indices. This strongly indicated nonsolar abundance ratios and has subsequently been confirmed [e.g. Worthey (1998); Tantalo & Chiosi (2004); Thomas et al. (2003); Proctor & Sansom (2002); Maraston et al. (2003)]. Trager et al. (2000a,b) introduced the valuable step of using synthetic stellar spectra (Tripicco & Bell 1995) to simulate the effects of abundance ratio changes in the integrated-light models.

Recently, Worthey (2004) used an updated version of Tripicco & Bell (1995), that is, Houdashelt et al. (2002), hereafter HTWB, to infer a chemical mixture for local group elliptical galaxy M32 for 10 elements: C, N, Mg, and Na were measured with some security, while Fe, O, Ca, Si, Cr, and Ti were more uncertain. The spectrum itself was not used directly. Rather, a set of 25 absorption feature indices on the Lick/IDS system (Worthey et al. 1994; Worthey & Ottaviani 1997) was utilized, so that the information extracted was limited to what these 25 numbers could yield.

The present work investigates this issue of measuring individual elements in the integrated light of passive stellar systems. How many elements could be measured *individually* if we had excellent spectra, excellent models, and could examine all wavelengths of interest? We outline our approach to answering this question in §2, then present results ordered by groups of elements, and finally summarize and conclude.

2. Analysis

High-resolution spectral abundance analysis on stars traditionally relies on a small set of transitions whose oscillator strengths and damping profiles are either known from laboratory work or are deduced through an analysis of the lines as they appear in the spectra of abundance standards, e.g., the Sun or Arcturus. Ideally, these lines will be in isolated patches of spectrum where no other lines exist to crowd the feature of interest. In many situations, however, interloper lines do affect the line under study, especially at blue or ultraviolet wavelengths and especially in cool stars. In these situations, the technique of spectral synthesis must be employed, where swaths of spectrum are computed that include many lines. Besides the atomic physics of the lines themselve, the other ingredient needed for good abundances is the stellar atmosphere (i.e., the relation of pressure, temperature and opacity with optical depth). Ideally, computing an accurate stellar atmosphere requires consideration of continuous and line opacity sources over the entire wavelength range from which flux emerges, so that spectral synthesis and the computation of the atmosphere are done simultaneously to iterate to the final atmosphere structure [Castelli & Kurucz (2004) and references therein]. A less computationally intensive approach (and the one adopted here) is to decouple the model atmosphere and synthetic spectra calculations. In this case, the model atmosphere is generated using pre-calculated line opacity "tables" (opacity distribution functions) for a given composition These basic principles are described in detail in Gustafsson et al. (1975)). The resulting run of temperature, pressure, opacity, and optical depth are used with an appropriate line-list to calculate the emergent flux over the wavelength range of interest.

Such spectral synthesis requires lists of all relevant atomic and molecular transitions, along with oscillator strengths and damping constants. Lines that are strong in the solar spectrum have largely been identified, but weak lines and many lines in the ultraviolet have not (Kurucz 1995). Individual molecular lines can be more problematic as line lists often include transitions derived from theory (due to a lack of laboratory values) which frequently are not as accurate as one would want for high resolution spectroscopy. However, the inclusion of theoretical molecular bands is often reasonable for overall opacity calculations. Many workers are constantly improving the available line lists.

Here we wish to use these spectral synthesis tools to study elliptical galaxy spectra. Such spectra are highly composite and are velocity broadened to as high as 350 km s^{-1} for the largest galaxies. At such large velocity dispersions, only the very strongest of lines are recognizable in the spectrum. All medium and weak lines are blended together and any true continuum is hopelessly lost. For spectral synthesis, this means that the weak, poorly characterized (or even perhaps unidentified) lines contribute strongly to the spectral shape. So at low spectral resolution (or high velocity dispersion), the mismatches between theory and real stars are obvious despite substantial improvements in line lists over the years.

We computed synthetic spectra of a giant (T_{eff} = 4250, log g = 1.90) and a main-sequence turnoff dwarf (T_{eff} = 6200, log g = 4.10), combined them, and broadened them to Gaussian σ of 200 km s^{-1} to simulate an elliptical galaxy. We then computed synthetic spectra (or used those of HTWB), for the same stars, increasing the abundance of a single element at a time. This was done for C, N, O, Na, Mg, Al, Si, S, K, Ca, Sc, Ti, V, Cr, Mn, Fe, Co, Ni, Cu, Zn, Sr, Ba, and Eu. Both the HTWB spectra and ours were calculated using MARCS model atmospheres (Gustafsson et al. 1975) and the program SSG (Bell et al. 1994). Spectra for the synthetic giant using both sources and for two K giants from the CFL library (Valdes et al. 2004) are plotted in Figure 1. HD 114092 is slightly cooler and more metal-rich than HD 102328. All spectra were smoothed to 200 km s^{-1}, corresponding to the velocity dispersion typical of a galaxy around L^*, the "knee" in the luminosity function of cluster galaxies [$\approx 0.9L^*$ according to the fit in Tonry (1985)]. The synthetic spectra do not match the observed stars perfectly, with easily detectable deviations. The two synthetic spectra do not match each other because of version mismatches between them (i.e. differences in assumed solar abundance, model atmosphere structure, code changes, and line lists), but neither has serious flaws in matching the continuum and the major spectral features. The remaining several-percent scatter is indicative of the absolute accuracy. Most important to the present work is that the differential effects caused by abundance changes should be independent of the Figure 1 scatter to a large extent.

For each model star the abundance of each elemental of interest was increased by 0.3 dex and a new spectrum calculated, except for C which was increased by 0.15 dex. This exception for carbon was inserted because a 0.3-dex enhancement of C relative to O causes the C/O ratio to approach 1, radically changing the molecular equilibrium so that the star begins to turn into a carbon star. These spectra were combined with equal contribution from the turnoff dwarf and giant at 5000 Å, approximately aping a $\sim$5 Gyr age stellar population [cf. Worthey (1994) or Buzzoni (1989) for the fractional contributions of light from different

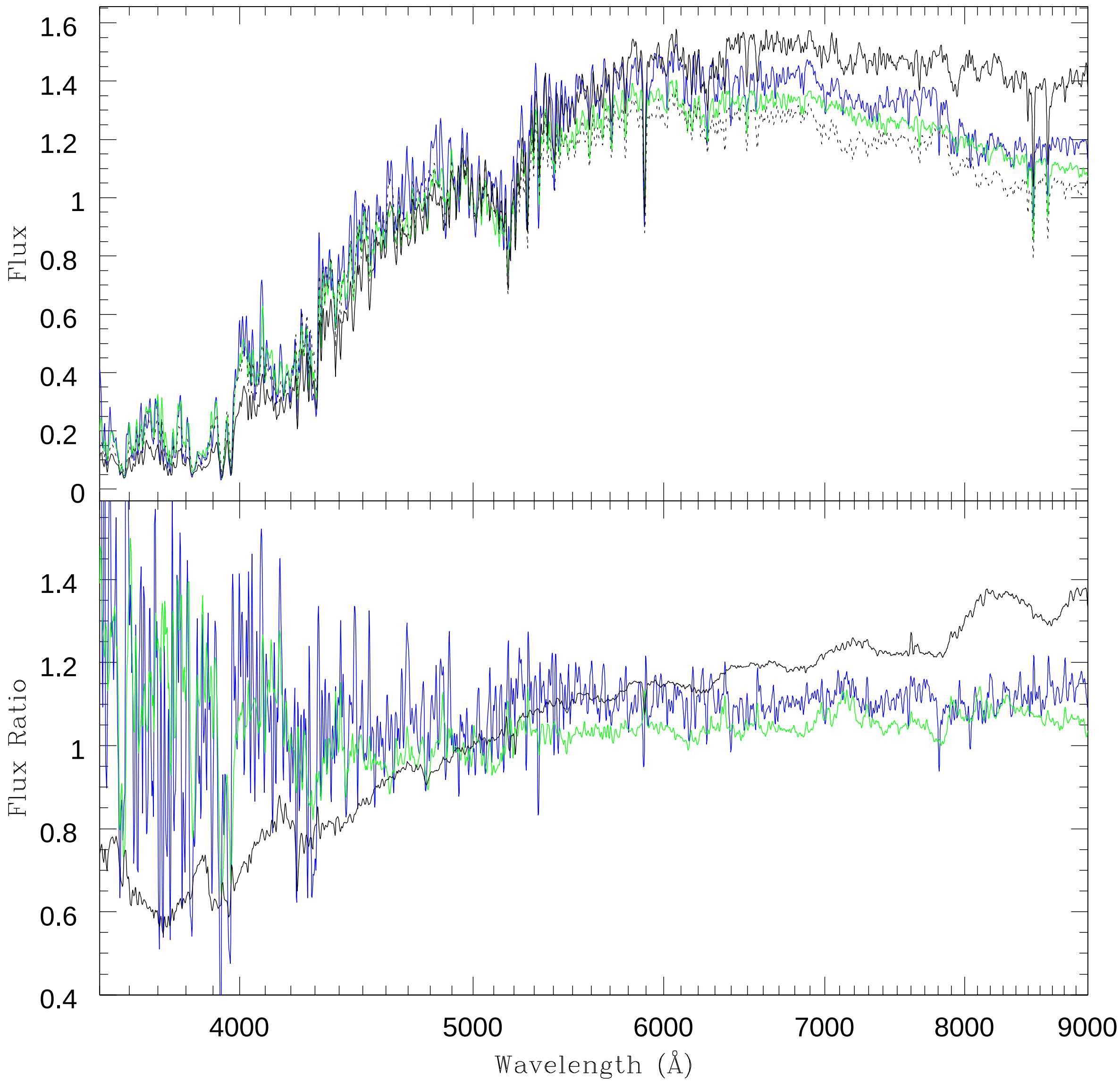

Fig. 1.— Observational and synthetic K giant spectra (F_λ, normalized at 5000Å). In the top panel the fluxes of HD 114092 (*solid black*) and HD 102328 (*dashed black*) from the CFL library (Valdes et al. 2004) are plotted along with the synthetic spectra of HTWB (*green*) and this work (*blue*). In the bottom panel the spectrum of HD 102328 is divided into the other three using the same color scheme.

stellar evolutionary phases]. This "galaxy" spectrum was broadened to a Gaussian σ of 200 km s^{-1} to simulate an elliptical galaxy somewhat more massive than the Milky Way. The procedure was repeated for each spectrum with an "enhanced abundance" of a particular element. For purposes of locating regions of spectrum that showed significant response to the abundance changes, we took the ratio of the enhanced "galaxy" spectrum and the unenhanced "galaxy" spectrum.

We then defined indices for interesting features consisting of three passbands in the Lick/IDS style. The central passband spans the absorption feature itself. The central passband is flanked by blue and red continuum passbands. A pseudocontinuum is defined by "drawing" a line between the wavelength midpoints and average flux values of the blue and red sides. The index itself is an equivalent width, integrating the difference of pseudocontinuum and flux over the index passband. Using these indices and assuming a photon error such that S/N = 100 around 5000 Å and proportional to $F_\lambda^{\frac{1}{2}}$, we determined index values and errors to gauge the feasibility of measuring individual elements in real galaxies.

3. Results

Absorption feature indices are a useful way of summarizing results since one can reduce spectral data to a single number plus its error. We list the features that we defined in Table 1. The index name is composed of the element or elements that the index targets, along with the center wavelength of the index passband. That is, the wavelengths in the names do not correspond to any actual atomic or molecular transitions, except by coincidence. Wavelengths are listed in units of Ångstroms.

For our "galaxy" the index measurements in Å of equivalent width are given in Table 2, column 2, and the error associated with S/N = 100 at 5000 Å is given in column 3. The remainder of the columns are the changes (enhanced minus unenhanced) in the index wrought by an element enhancement of 0.3 dex (or 0.15 dex for C) in units of the error of column 3. The final column gives the result for a bulk enhancement of 0.3 dex for all heavy elements (including C). HTWB spectra were used for elements C, N, O, Na, Mg, Si, Ca, Ti, Fe, Cr, and our own for the rest.

Table 1. Index Definitions

Index Band	Blue Continuum	Red Continuum	Name
4626.4 — 4743.3	4557.3 — 4589.5	4805.1 — 4835.3	CO4685
5154.3 — 5167.3	5108.4 — 5138.8	5188.4 — 5202.0	CO5161
3840.3 — 3883.4	3768.1 — 3812.3	3896.4 — 3916.2	CNO3862
4129.4 — 4219.8	4082.5 — 4123.3	4243.3 — 4284.2	CNO4175
8167.4 — 8212.5	8081.8 — 8137.2	8231.6 — 8289.7	Na8190
3823.4 — 3847.6	3754.7 — 3782.0	3850.0 — 3865.0	Mg3835
4760.8 — 4798.8	4738.9 — 4757.3	4819.8 — 4835.5	Mg4780
3937.6 — 3967.4	3921.3 — 3935.5	3969.5 — 3987.0	Al3953
4093.3 — 4107.8	4057.9 — 4075.3	4111.5 — 4131.0	Si4101
4490.8 — 4534.6	4448.7 — 4487.6	4541.1 — 4572.7	Si4513
4035.9 — 4047.5	4014.9 — 4029.0	4054.7 — 4070.4	K4042
3899.5 — 4003.5	3806.5 — 3833.8	4020.7 — 4052.4	CaHK
8525.9 — 8558.3	8452.4 — 8482.3	8566.8 — 8595.0	Ca8542
8648.8 — 8676.1	8601.0 — 8635.1	8703.4 — 8742.6	Ca8662
4680.6 — 4704.4	4652.2 — 4677.3	4717.6 — 4737.7	S4693
3604.9 — 3620.4	3539.7 — 3563.2	3676.8 — 3697.4	Sc3613
4303.0 — 4320.7	4286.1 — 4300.6	4335.8 — 4354.4	Sc4312
6265.1 — 6318.8	6199.2 — 6231.1	6320.9 — 6366.5	Sc6292
4283.6 — 4308.2	4253.8 — 4274.4	4324.5 — 4343.0	Ti4296
4525.3 — 4541.1	4486.3 — 4506.2	4548.7 — 4561.3	Ti4533
4973.1 — 5026.1	4930.6 — 4959.4	5035.4 — 5052.5	Ti5000
4086.4 — 4138.5	4057.1 — 4074.3	4145.0 — 4160.5	V4112
4919.6 — 4937.4	4899.8 — 4914.8	4951.8 — 4965.2	V4928
6592.2 — 6615.4	6516.5 — 6549.7	6655.8 — 6693.8	V6604
3586.6 — 3602.4	3536.6 — 3560.5	3625.2 — 3641.5	Cr3594
4246.8 — 4281.3	4179.3 — 4195.6	4310.7 — 4334.7	Cr4264
5198.9 — 5213.6	5130.0 — 5149.2	5240.3 — 5257.0	Cr5206
3780.9 — 3806.1	3744.9 — 3769.6	3847.9 — 3865.3	Mn3794
3992.6 — 4044.4	3940.9 — 3962.3	4096.3 — 4121.5	Mn4018
4443.3 — 4477.7	4386.8 — 4406.9	4506.1 — 4530.3	Mn4061
4741.5 — 4773.4	4715.6 — 4737.8	4792.4 — 4812.1	Mn4757
4037.9 — 4078.4	4009.0 — 4031.1	4107.6 — 4125.7	Fe4058
4907.0 — 4943.8	4894.5 — 4907.0	4943.8 — 4954.5	Fe4930
3695.0 — 3708.0	3656.0 — 3676.1	3712.4 — 3723.0	Co3701
3831.4 — 3849.3	3772.7 — 3810.2	3850.4 — 3863.4	Co3840
3864.5 — 3887.0	3850.4 — 3863.4	3909.3 — 3934.4	Co3876
7781.9 — 7845.5	7723.0 — 7777.2	7847.6 — 7870.2	Co7815
8162.8 — 8207.5	8102.0 — 8142.9	8214.1 — 8255.0	Co8185
3655.1 — 3679.4	3630.4 — 3646.6	3685.4 — 3705.3	Ni3667
3766.1 — 3794.7	3749.4 — 3764.4	3800.1 — 3815.6	Ni3780
4279.6 — 4305.4	4260.9 — 4275.3	4307.4 — 4323.6	Ni4292
4897.4 — 4922.1	4879.3 — 4895.8	4953.2 — 4969.4	Ni4910
4966.0 — 4986.3	4951.5 — 4964.4	5016.8 — 5028.9	Ni4976
5578.3 — 5605.4	5521.1 — 5542.7	5612.6 — 5632.6	Ni5592
5209.1 — 5225.3	5160.9 — 5186.9	5247.5 — 5275.8	Cu5217
5772.3 — 5787.3	5720.1 — 5753.2	5808.0 — 5830.8	Cu5780
4708.7 — 4731.5	4652.7 — 4670.0	4755.4 — 4775.5	Zn4720
4545.4 — 4558.5	4522.2 — 4535.0	4559.5 — 4578.8	Ba4552
4922.8 — 4943.3	4902.7 — 4916.1	4967.2 — 4992.7	Ba4933
6130.7 — 6152.6	6105.8 — 6128.2	6176.3 — 6209.6	Ba6142
4069.0 — 4082.2	4038.4 — 4055.6	4105.3 — 4126.8	Sr4076
3962.8 — 3976.7	3929.0 — 3945.8	3980.7 — 3993.9	Eu3970
4584.8 — 4598.8	4533.5 — 4550.8	4626.3 — 4645.7	Eu4592

Table 2. Spectral Responses to Element Enhancements for New Indices

Name	I_O (Å)	σ (Å)	C	N	O	Na	Mg	Al	Si	S	K	Ca	Sc	Ti	V	Cr	Mn	Fe	Co	Ni	Cu	Zn	Sr	Ba	Eu	×2
CO4685	1.087	0.255	11.84	-1.08	-4.53	0.03	-0.09	-0.01	-2.71	0.16	0.00	-0.37	-0.05	-0.16	0.07	-0.43	-0.15	0.77	-0.12	0.40	0.00	0.48	-0.36	-0.29	0.00	5.1
CO5161	0.650	0.059	5.51	0.10	-3.32	-0.05	1.27	-0.03	-0.59	0.00	0.00	-0.19	0.00	-0.78	0.02	-0.98	-0.19	-0.75	0.08	0.64	0.00	0.00	0.05	0.36	0.02	1.7
CNO3862	5.710	0.161	5.03	15.30	-3.22	0.05	2.67	-0.04	-2.35	0.01	0.00	-6.52	-0.08	-0.83	0.63	0.86	0.16	-3.81	0.17	-0.17	0.00	0.00	0.00	-0.06	0.01	11.4
CNO4175	3.606	0.224	7.43	6.67	-6.05	-0.33	-0.93	0.00	0.76	-0.01	0.00	-0.78	0.17	0.21	-1.11	-1.94	-0.43	-1.52	-0.18	-0.04	0.00	0.00	0.32	0.21	0.00	2.3
Na8190	-0.745	0.129	-0.10	-0.12	0.10	1.26	-0.12	-0.02	0.02	-0.02	-0.02	0.32	0.00	-0.08	-0.23	-0.09	0.00	-2.75	2.22	-0.01	0.00	0.00	0.00	0.09	0.00	-1.4
Mg3835	6.238	0.113	0.34	-3.73	1.42	0.06	5.05	0.00	0.29	0.03	0.00	-0.19	0.01	-0.64	-0.73	-0.91	1.33	3.41	0.99	-0.41	0.00	0.00	0.00	0.00	0.03	0.6
Mg4780	0.580	0.124	0.08	0.00	0.81	-0.61	3.24	0.00	-0.01	-0.01	0.00	-0.25	-0.56	0.46	-0.24	0.28	-0.26	0.56	0.10	-0.05	0.00	0.00	-0.52	0.00	0.00	0.8
Al3953	-3.608	0.183	1.73	-0.02	0.21	0.07	0.32	4.56	0.09	-0.01	0.00	-0.05	-0.03	-0.46	0.39	-0.47	-0.27	-0.64	0.31	-0.05	0.00	0.00	0.00	0.00	-0.11	0.5
Si4101	1.186	0.074	-1.86	0.01	-0.11	-0.12	-0.39	-0.01	2.45	0.01	-0.01	0.51	0.01	-1.12	1.34	-0.42	-0.41	-2.80	-0.09	-0.42	0.00	0.00	-0.46	-0.03	-0.05	-1.0
Si4513	-2.273	0.128	-1.38	0.73	-0.34	-0.18	-1.14	0.01	3.88	0.00	0.00	-0.60	-0.12	0.22	-0.57	-0.45	-0.53	-0.69	-0.02	0.41	0.01	0.01	0.01	-1.36	0.01	-1.6
S4693	-0.868	0.087	3.45	0.01	-1.59	-0.05	0.33	0.02	-0.43	0.47	0.00	0.23	0.11	-0.05	-0.24	0.48	-0.08	-1.67	-0.54	0.20	0.00	-0.41	-0.10	0.03	-0.08	1.6
K4042	0.438	0.065	-3.09	-0.09	0.15	-0.06	-0.29	-0.02	0.02	0.00	0.43	-0.57	0.32	-1.09	0.05	0.34	-1.12	1.00	-0.05	-0.51	0.00	0.00	-0.05	0.00	0.00	0.3
CaHK	17.653	0.271	3.42	-3.21	1.66	-0.41	-5.15	2.20	-2.15	-0.01	-0.21	29.43	-0.64	1.10	0.14	-0.15	-2.34	-9.05	0.86	-0.06	0.00	0.00	-0.01	0.04	0.12	7.0
Ca8542	3.132	0.110	1.63	0.10	0.02	-0.47	-2.29	0.00	-0.76	-0.01	0.00	11.24	0.00	0.14	0.00	0.05	0.00	-2.50	-0.01	0.02	0.00	0.00	0.00	0.27	0.00	5.7
Ca8662	1.777	0.097	0.96	0.05	0.04	-0.29	-2.00	-0.01	-0.79	0.21	0.00	8.43	0.00	-0.22	0.00	-0.10	0.00	-1.15	0.01	0.00	0.00	0.00	0.00	-0.03	0.00	4.6
Sc3613	3.539	0.083	4.40	-1.83	2.04	-0.06	-0.84	-0.02	0.02	0.00	0.00	-0.19	1.88	-1.18	-0.70	0.53	-0.04	5.28	-0.02	-0.27	0.00	0.00	0.00	0.00	0.01	2.0
Sc4312	-2.154	0.101	1.14	0.04	-0.66	-0.15	-0.87	0.02	-0.57	0.00	0.00	0.09	1.20	-0.31	0.02	-1.18	-0.02	0.72	-0.02	-1.05	0.00	0.00	0.00	-0.06	0.00	0.0
Sc6292	0.445	0.132	-0.11	-0.33	0.10	-0.01	0.07	0.17	-0.08	0.00	0.00	-0.10	1.36	-0.06	-0.25	-0.27	0.00	-0.18	-0.03	-0.28	0.00	-0.02	-0.02	-0.08	0.00	0.0
Ti4296	6.097	0.086	9.85	0.23	-1.53	-0.33	-1.13	-0.03	-2.02	0.00	0.00	1.23	0.23	2.90	0.23	-0.83	-0.38	-2.57	0.03	1.48	0.00	0.00	0.00	-0.01	-0.01	3.1
Ti4533	-0.106	0.075	1.21	0.16	-0.01	-0.05	0.01	0.00	0.07	0.00	0.00	0.20	0.00	2.21	0.64	0.41	-0.23	0.49	0.37	-0.16	0.00	0.00	0.00	-2.32	0.00	2.9
Ti5000	1.682	0.154	0.76	0.03	0.99	0.23	-0.61	0.00	-0.01	0.01	0.00	0.12	-0.31	2.76	-0.03	-0.27	0.01	0.77	0.00	0.74	0.00	0.00	-0.05	-0.56	0.00	2.9
V4112	-0.708	0.203	-3.32	-0.51	0.81	0.08	0.28	0.00	2.18	0.01	0.00	0.42	-0.08	-1.27	1.67	0.42	-0.57	-3.97	-0.05	0.25	0.00	0.00	-0.83	-0.02	0.06	-1.8
V4928	1.348	0.072	1.88	0.03	-0.69	-0.01	-0.24	0.00	-0.07	0.00	0.00	0.03	-0.26	0.39	0.81	0.40	-0.26	0.68	-0.01	-0.29	0.00	0.00	-0.15	1.96	0.00	2.0
V6604	0.222	0.078	0.46	-0.21	0.17	-0.03	-0.10	-0.15	-0.14	0.00	0.00	-0.21	0.03	0.01	1.26	-0.04	0.00	0.85	0.19	0.03	0.00	0.00	-0.01	-0.15	0.00	0.8
Cr3594	-0.159	0.105	2.07	-0.18	1.13	0.04	-0.05	0.01	0.04	0.01	0.00	0.16	0.05	0.50	0.48	2.76	-0.20	-1.50	-0.02	0.70	0.01	0.01	0.01	0.01	-0.04	1.5
Cr4264	2.224	0.122	-1.01	-2.89	2.64	-0.02	-0.23	-0.02	0.58	0.01	0.01	-0.36	-0.37	0.09	-0.31	3.52	0.66	1.82	0.07	0.12	0.00	0.00	0.00	0.00	0.02	1.4
Cr5206	0.932	0.063	-2.78	0.02	1.67	-0.24	1.24	0.00	-0.03	0.00	0.00	0.11	-0.13	0.24	-0.03	3.98	0.00	-1.25	-0.73	-0.08	0.16	0.00	0.00	0.00	0.00	1.5
Mn3794	-0.551	0.140	0.73	-2.16	-0.93	0.14	1.89	-0.01	0.69	-0.01	0.00	-0.01	0.00	-1.57	-0.44	-0.58	0.74	-1.86	-0.04	0.29	0.00	0.00	0.00	0.00	-0.03	-3.9
Mn4018	18.467	0.251	-5.11	-2.37	0.81	0.31	1.06	-3.70	-0.51	0.00	0.12	13.60	0.36	1.29	-1.74	0.46	2.14	5.67	-0.18	0.10	0.00	0.00	0.01	0.00	0.00	-6.9
Mn4061	-1.047	0.118	0.12	-0.57	2.04	0.24	1.83	0.02	-2.43	0.00	0.00	1.12	-0.22	0.31	0.58	0.69	1.43	1.31	-0.13	-0.30	0.00	0.00	0.00	-0.04	0.00	1.5
Mn4757	1.149	0.102	-4.58	-0.05	1.95	0.31	1.03	0.01	0.43	0.00	0.00	0.03	0.22	-0.05	0.12	0.59	1.75	0.51	-0.06	0.28	0.00	-0.61	-0.20	-0.03	0.00	-0.4
Fe4058	3.103	0.139	-1.28	-1.01	1.25	0.00	0.38	-0.06	-1.37	-0.01	0.18	-1.61	0.14	-0.24	-0.60	0.01	-0.27	6.58	0.14	-0.96	-0.01	0.00	1.49	-0.01	-0.04	2.9
Fe4930	3.011	0.126	3.10	0.05	-0.22	-0.09	-0.32	0.00	-0.30	0.00	0.01	-0.06	-0.38	0.87	0.35	-0.02	0.00	3.25	-0.02	1.14	0.00	0.00	-0.02	0.88	0.00	4.1
Co3701	0.141	0.101	1.07	-0.03	-0.19	0.06	0.45	-0.01	0.06	-0.01	0.00	0.39	-0.15	0.16	0.44	-0.46	0.19	-0.37	0.91	-0.53	0.00	0.00	0.00	0.00	0.00	1.0
Co3840	2.865	0.103	0.37	-2.52	0.38	0.02	3.57	0.01	0.20	0.02	0.00	-0.15	0.01	-0.35	-0.49	-0.82	1.08	1.07	1.09	-0.42	0.00	0.00	0.00	0.00	0.03	-0.0
Co3876	0.493	0.137	1.11	2.72	-0.28	0.02	0.77	-0.01	-0.35	0.02	0.00	-4.27	-0.02	0.00	-0.28	-0.27	-0.05	0.11	1.05	-0.31	0.00	0.00	0.00	0.01	-0.01	2.0
Co7815	1.750	0.173	-0.37	-0.33	0.24	0.03	0.05	0.37	-0.03	0.01	0.00	0.19	0.02	-0.08	0.01	-0.05	0.01	0.10	4.08	0.03	0.00	0.00	0.00	0.00	0.00	0.1
Co8185	-0.616	0.135	-0.28	-0.18	0.15	1.21	-0.16	-0.01	-0.04	-0.01	-0.02	0.37	0.00	-0.11	-0.21	-0.04	-0.01	-2.75	2.26	-0.01	0.00	0.00	0.00	0.04	0.00	-1.6
Ni3667	-0.198	0.137	0.74	-0.16	-0.40	0.04	0.87	0.01	0.04	0.01	0.00	0.12	0.38	-1.09	-0.85	-0.17	0.02	-3.49	-0.59	0.87	0.00	0.00	0.00	0.00	-0.01	-2.3
Ni3780	-1.444	0.161	3.90	-0.03	-1.30	0.07	1.29	0.01	0.24	-0.01	0.01	-0.01	0.00	-2.58	-0.21	0.07	0.00	-3.34	-0.22	1.13	0.00	0.00	0.00	0.00	-0.02	-2.8
Ni4292	5.651	0.095	5.76	0.14	-0.92	-0.26	-0.55	-0.03	-0.89	0.00	0.00	0.85	-0.47	2.24	0.38	-0.40	-0.15	-2.85	0.06	1.56	0.00	0.00	0.00	0.00	-0.01	1.4
Ni4910	1.652	0.090	0.79	-0.01	-0.43	0.02	0.12	0.00	-0.16	-0.01	0.00	-0.02	0.18	-0.32	-0.04	-0.78	-0.26	0.97	0.01	1.73	0.00	0.00	-0.20	0.13	0.00	-0.3
Ni4976	0.536	0.087	0.94	0.01	0.20	0.31	0.46	0.01	0.18	0.00	0.00	-0.10	-0.37	0.95	0.00	-0.08	-0.31	-1.85	0.00	1.87	0.00	0.00	-0.24	0.00	0.00	1.2
Ni5592	0.285	0.093	0.98	-0.05	-0.03	0.02	-0.18	0.01	0.01	0.00	0.00	1.52	-0.01	-0.06	-0.03	0.20	-0.17	-0.83	-0.05	1.97	0.00	0.00	-0.06	-0.03	0.00	0.5
Cu5217	-1.717	0.073	-2.26	-0.10	0.84	0.36	-4.77	0.03	0.56	0.00	0.00	0.05	-0.01	0.89	0.01	1.32	0.00	0.70	-0.48	0.03	0.84	0.00	0.18	-0.03	0.00	-1.9
Cu5780	0.409	0.058	0.81	0.09	0.02	-0.03	0.07	0.00	0.28	0.00	0.00	-0.14	-0.10	0.36	0.09	1.50	0.10	0.19	-0.10	-0.10	0.79	0.00	0.00	0.02	0.00	2.7
Zn4720	-0.048	0.086	2.67	0.03	-1.79	-0.02	-0.78	-0.02	-0.37	0.00	0.00	0.06	0.12	-0.64	0.29	-0.98	-0.76	-1.31	0.42	0.41	0.00	0.95	0.12	0.03	-0.09	0.4
Ba4552	1.456	0.057	1.28	0.18	-0.09	0.18	0.00	0.00	-1.11	0.00	0.00	-0.30	-0.19	0.23	-0.37	0.26	-0.05	0.65	-0.32	-0.04	0.00	0.00	0.00	3.79	0.00	0.6
Ba4933	0.524	0.084	0.52	0.00	-0.61	-0.07	-0.46	0.00	-0.04	0.01	0.00	0.04	-0.13	-0.31	0.68	0.60	-0.04	-0.39	0.00	-1.27	0.00	0.00	0.00	1.87	0.00	0.0
Ba6142	0.777	0.078	1.40	-0.04	-0.86	0.06	-0.17	-0.03	0.23	0.00	0.00	-0.62	-0.05	0.06	0.46	0.05	0.00	1.95	0.00	-0.60	0.00	0.00	0.00	1.78	0.00	0.8
Sr4076	0.515	0.069	1.33	-0.58	0.91	0.03	0.12	0.00	-0.75	0.00	-0.16	-0.26	-0.36	0.83	-0.72	-0.41	-0.19	2.12	0.33	-0.25	0.00	0.00	3.86	0.00	-0.01	0.7

Ultimately, we aim to intercompare models and galaxy spectra to estimate (1) the bulk population age and metallicity [M/H] and (2) individual abundance ratios. The error analysis will be an overconstrained, least squares minimization problem, but we can illustrate the basic error propagation by considering a system of two indices that we measure to estimate two abundance ratios. Age and metallicity must also be estimated, but we assume this is done with other indices in the following example. Suppose the $n^{\rm th}$ index can be represented by terms

$$I_n = I_{n,AM} + \Big[\sum_k J_{nk}\tilde{Z}_k\Big]\sigma_n \tag{1}$$

where n is the index for the Lick-style index and k is the index over elements. I_n is the measured index, but $I_{n,AM}$ is the index value for a scaled solar abundance distribution at the appropriate age (A) and metallicity (M) for the stellar population. J_{nk} is the index response from Table 2 or Table 3. Because the table entries are in units of photon noise σ per 0.3 dex (0.15 dex for C) abundance change, we define $\tilde{Z}_k \equiv$[Z_k/M]/0.3 dex, or, for Carbon, $\tilde{Z}_6 =$[C/M]/0.15 dex. Finally, σ_n are the Table 2 or 3 column 3 entries.

For a system of two indices, the solution for two abundances is:

$$\tilde{Z}_1 = (J_{12}J_{21} - J_{11}J_{22})^{-1}[J_{12}\frac{I_2 - I_{2,AM}}{\sigma_2} - J_{22}\frac{I_1 - I_{1,AM}}{\sigma_1}] \tag{2}$$

$$\tilde{Z}_2 = (J_{12}J_{21} - J_{11}J_{22})^{-1}[J_{21}\frac{I_1 - I_{1,AM}}{\sigma_1} - J_{11}\frac{I_2 - I_{2,AM}}{\sigma_2}] \tag{3}$$

One can write the Gaussian-random errors for the abundances by inspection. Assuming that (1) the error due to getting the wrong age-metallicity model σ_{AM} is negligible and that (2) the measured index error is the same as the tabulated photon-derived error σ_n, the abundance errors are:

$$\sigma_{\tilde{Z}_1} =\mid (J_{12}J_{21} - J_{11}J_{22})^{-1} \mid [J_{12}^2 + J_{22}^2]^{\frac{1}{2}} \tag{4}$$

$$\sigma_{\tilde{Z}_2} =\mid (J_{12}J_{21} - J_{11}J_{22})^{-1} \mid [J_{21}^2 + J_{11}^2]^{\frac{1}{2}} \tag{5}$$

These equations can be used to test the separability of abundance measurements for pairs of species. For example, suppose one wanted to measure species C ($k = 1$) and Mg ($k = 2$) with indices CN_1 ($n = 1$) and Mg_1 ($n = 2$). Then, from Table 3, the J_{nk} become:

Table 2—Continued

Name	I_O (Å)	σ (Å)	C	N	O	Na	Mg	Al	Si	S	K	Ca	Sc	Ti	V	Cr	Mn	Fe	Co	Ni	Cu	Zn	Sr	Ba	Eu	$\times 2$
Eu3970	5.364	0.066	2.26	0.23	0.42	-0.11	-0.55	0.09	-1.21	0.02	0.00	9.92	0.00	-0.68	-0.02	-0.36	0.26	-1.83	-0.35	0.48	0.00	0.00	0.00	0.00	0.67	4.55
Eu4592	0.348	0.063	-0.71	-0.11	0.46	-0.17	-0.25	-0.02	0.49	0.00	0.00	0.25	0.02	-1.78	0.71	0.51	0.00	1.25	-0.16	0.43	0.00	-0.03	0.00	-0.51	0.56	-0.51

$J_{11} = 6.50$, $J_{12} = -0.50$, $J_{21} = 15.50$, and $J_{22} = 14.50$. Then $\sigma_{\tilde{Z}_1} = 0.14$ and $\sigma_{\tilde{Z}_2} = 0.16$, or $\sigma_{[\mathrm{C/M}]} = 0.15\sigma_{\tilde{Z}_1} = 0.021$ and $\sigma_{[\mathrm{Mg/M}]} = 0.30\sigma_{\tilde{Z}_2} = 0.045$. These errors are larger than those that one would infer from Table 3 because of the covariances. I.e., computed in dex by taking 0.3 (or 0.15) and dividing it by the tabulated response, $\sigma_{[\mathrm{C/M}]} = 0.023$ (from $\mathrm{CN_1}$) or 0.010 (from $\mathrm{Mg_1}$) and $\sigma_{[\mathrm{Mg/M}]} = 0.600$ (from $\mathrm{CN_1}$) or 0.021 (from $\mathrm{Mg_1}$).

Some indices defined for weak-lined elements such as Cu have tabulated responses for other elements that are stronger than the signal for the targeted element. One might worry that the strong presence of other elements (such as Fe) might obliterate the measurement of [Cu/M], for example, but this fear is not borne out because the response of most non-Cu indices is zero for Cu. Using Fe4058 and Cu5217 to measure Fe and Cu, for instance, yields $\sigma_{[\mathrm{Fe/M}]} = 0.044$ and $\sigma_{[\mathrm{Cu/M}]} = 0.349$ using the equations above, and almost identical values for inverting the Table 2 values directly for the Fe or Cu abundances, respectively.

3.1. C, N, O

In cool stars and elliptical galaxies C, N, and O are manifested in the spectrum almost exclusively through molecular species such as NH, CN, C_2, CH, and CO. CO has the highest dissociation energy, and since O is typically the most abundant of the three elements, most of the carbon is incorporated into CO molecules. The three elements are linked together via the molecular equilibrium balancing. The usual effect, illustrated in Figure 2, is that O behaves like anti-CN since adding O will decrease the amount of available C by incorporating more C into CO molecules. Figure 3 and subsequent figures show the division of an altered, single-element-enhanced spectrum by the unaltered spectrum. Carbon abundance is up only 0.15 dex, but all other elements are up 0.3 dex.

It should be possible to disentangle O from C and N by using features such as the Lick/IDS index $C_2$4668 that is mostly sensitive to C abundance and the indices CO5161 and CO4685 that are insensitive to N. Neither the NH features at 3300 Å nor the CO bands at 2.3 μm are modeled here, but presumably are also beneficial. The spectral response to CNO changes are very easy to measure (many σ at S/N = 100). The only reservation is that molecular line lists are even more immature than atomic line lists, so precise models may be difficult to produce.

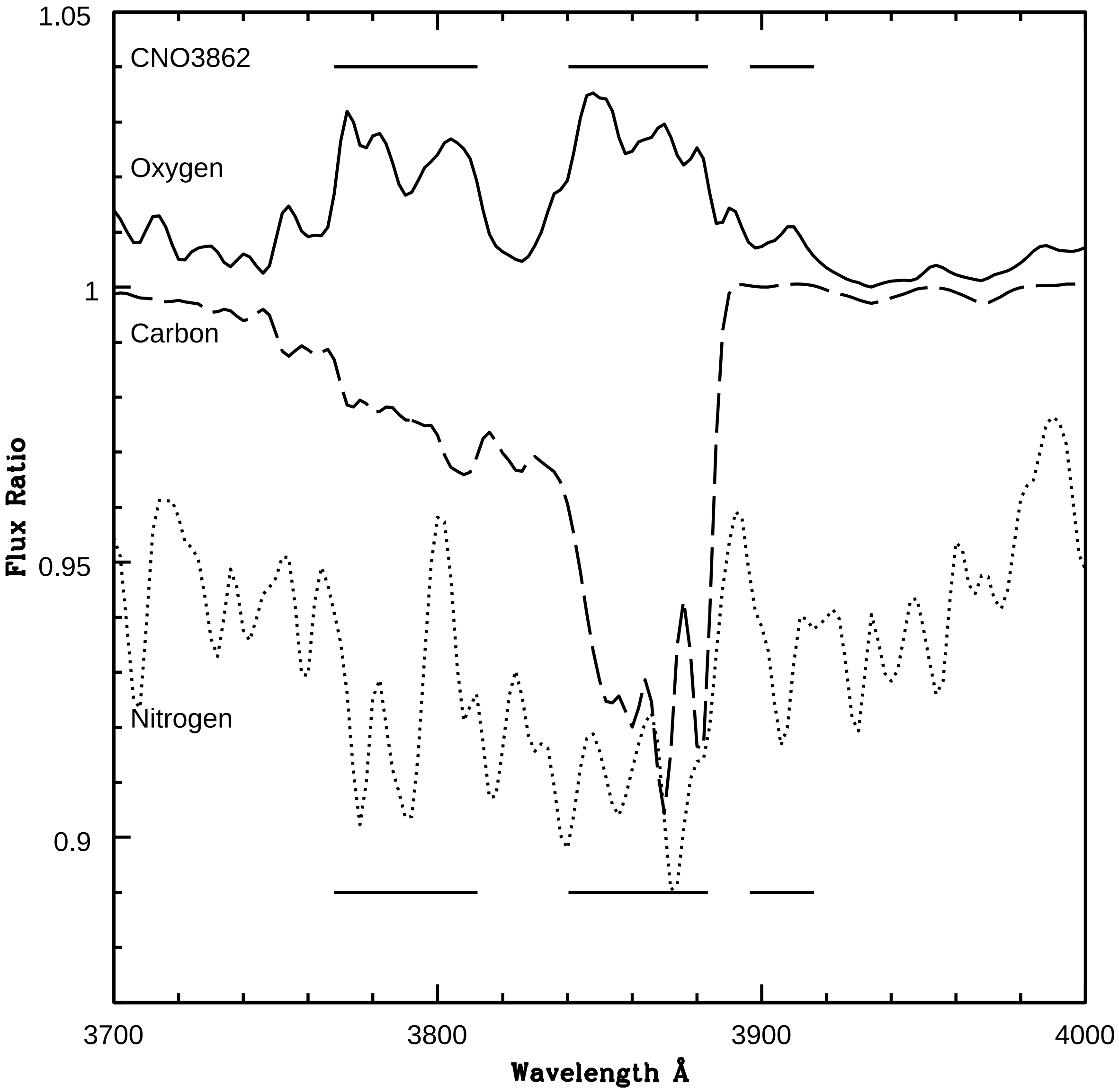

Fig. 2.— The CNO3862 index definition (*horizontal lines*). The relative spectral responses due to increased oxygen (*solid*), carbon (*dashed*), and nitrogen (*dotted*) abundances are also shown in the same spectral region.

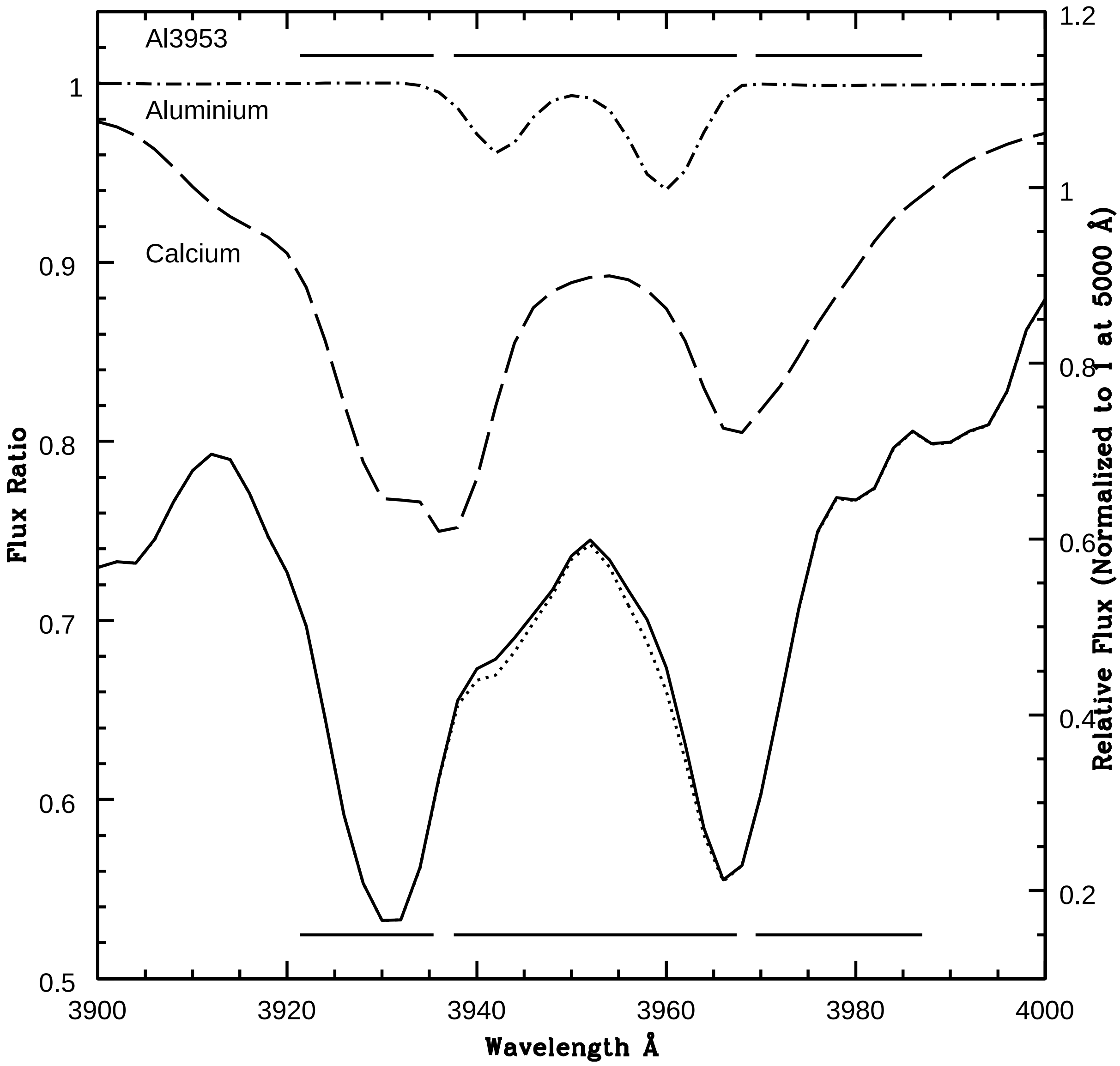

Fig. 3.— The Al3953 index definition (*horizontal lines*). The Al-enhanced (*dotted*) and normal (*solid*) spectra are overplotted near the bottom. The ratio spectra for Al-enhanced and Ca-enhanced models are shown toward the top.

3.2. Ca, Al

In the atmospheric window, only two aluminum transitions are found. There is a resonance line at λ3944.01 and one additional line at λ3961.52 (Meggers et al. 1975). Both are strong enough to be measured in 200 km s^{-1} spectra, but both are situated between the giant Fraunhofer lines of Ca II at λ3933.66 (K) and λ3968.47 (H). Jaschek & Jaschek (1995) indicate an equivalent width of the Al resonance line of about half an Ångstrom in G stars, as opposed to about 15 Å for the Ca K line. We illustrate the situation in Figure 3, where enhancements due to both Al and Ca are shown to the same scale. Spectral changes due to Ca are about 5 times larger than those due to Al, but the Al signature is clearly seen since the wavelength separation is significant.

The continuum passbands of the Al3953 index were tuned until the influence of Ca abundance changes summed to nearly zero. We did this in order to demonstrate to ourselves that it could easily be done, and to illustrate that it would be straightforward to separate effects due to Ca from effects due to Al. For this spectral region, one would probably want a spectral-synthesis approach rather than a feature-index approach. For instance, the cores of the H and K lines can be filled with emission from active stellar chromospheres, but also may suffer interstellar contamination since they are resonance lines. So the cores of H and K should be treated with more caution than we give to them in this exploratory paper. Even with all of these caveats, a 0.3-dex enhancement of Al produces a 4.5-σ effect in the spectrum. Calcium is easy to measure via the H and K lines (index CaHK), but also via the so-called "triplet" represented in Table 2 by indices Ca8542 and Ca8662, and by the Lick index Ca4227.

3.3. Na, Mg, Si

Sodium is easily measurable only via the Na D feature. The next best candidate is the Na doublet measured with index Na8190, but its spectral response is only a little better than 1-σ, as opposed to the 9-σ response of the Na D index. Also, both Fe and Co have significant features around 8190Å, adding to the uncertainty in measuring the Na abundance (cf. the very similar Co8185 index). The Na D index is less than desirable because of possible interstellar absorption in the Na D resonances, although many galaxies will redshift beyond the influence of the Galactic Na absorption, which is of order a few tenths of an Å in equivalent width (Welty et al. 1994).

Magnesium is easily measured from Lick/IDS indices Mg_1, Mg_2, and Mg b, but we also present alternative indices Mg3835 and Mg4780 (the weaker of the two). Mg4780 is

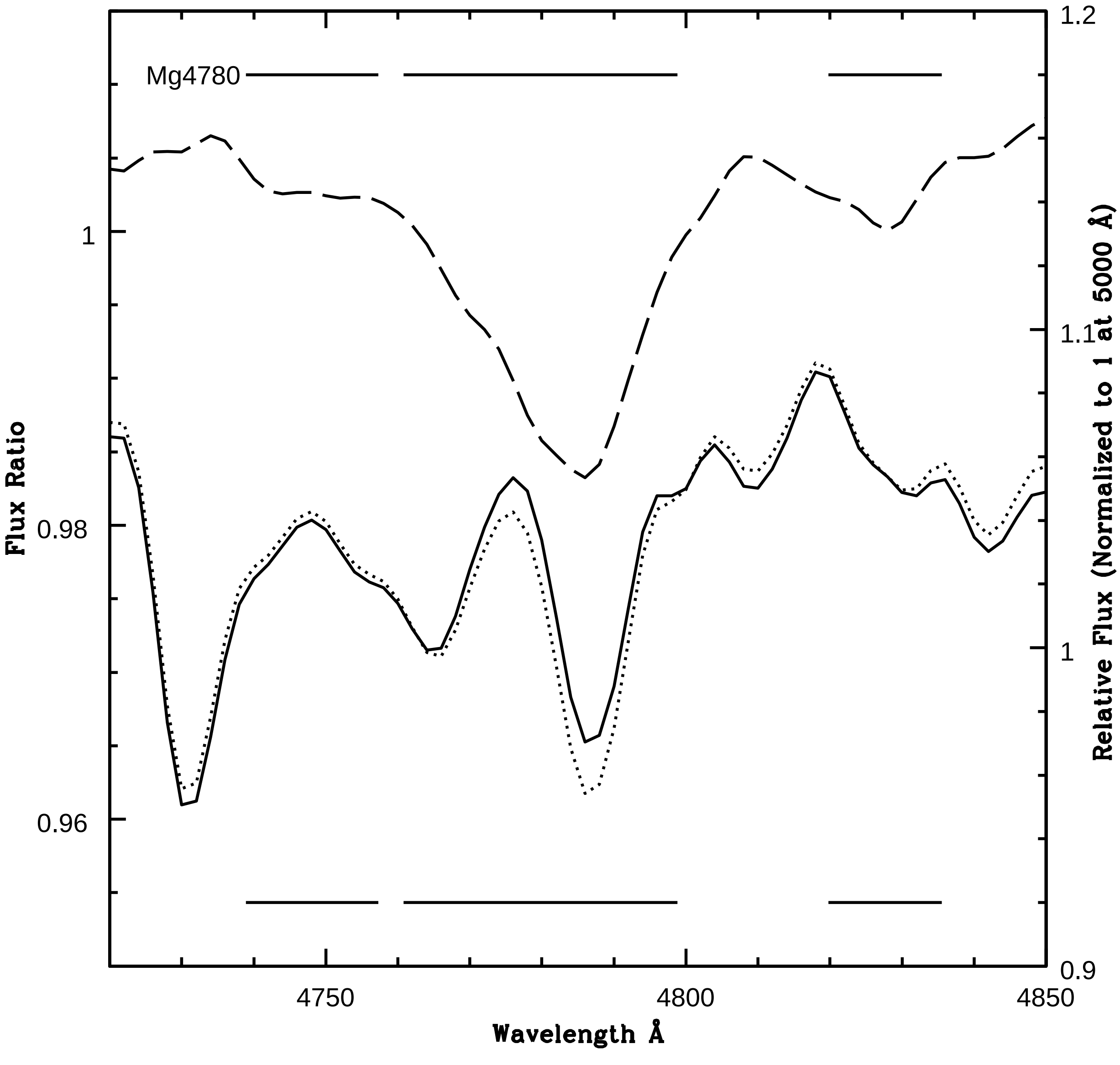

Fig. 4.— The Mg4780 index definition (*horizontal lines*). The Mg-enhanced (*dotted*) and normal (*solid*) spectra are overplotted near the bottom with scale to the right. The ratio of the two spectra are shown (*dashed*) at the top, with scale to the left.

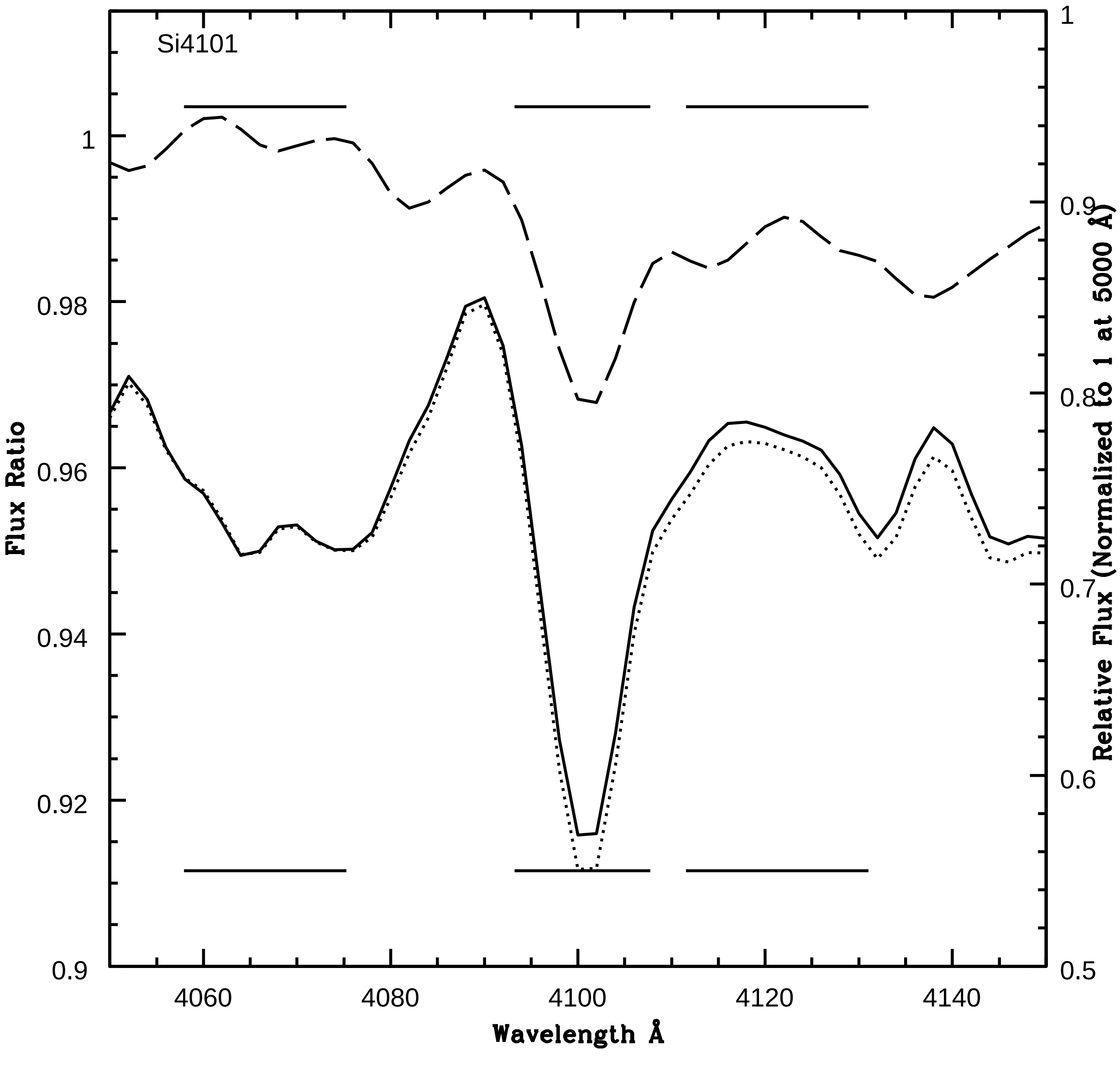

Fig. 5.— The Si4101 index definition (*horizontal lines*). The Si-enhanced (*dotted*) and normal (*solid*) spectra are overplotted near the bottom with scale to the right. The ratio of the two spectra are shown (*dashed*) at the top, with scale to the left.

illustrated in Figure 4.

The Si4101 index measures an atomic line at λ4102.94 and also lines due to SiH. It is illustrated in Figure 5. The well-studied line of Si II at λ4128.07 is weak in cool stars and so does not contribute substantially to the spectral shape. The Si4513 index appears to measure mostly SiH. Both Si4101 and Si4513 indices are relatively clean in the sense that other elements have little influence on the spectral shape for these indices, so the strength of these indices should be given by only three parameters (age, metallicity, and Si abundance) in real galaxies.

3.4. S, K

Neither sulfur nor potassium have much influence on the spectra of cool stars. Table 2 lists indices that measure the strongest blips in the spectrum, K4042 and S4693. Both of these indices seem to require S/N of 500 or more before K or S abundances can be reliably measured.

3.5. Cr, Mn, Fe, Ni

This group of elements has a problem opposite that of S and K; these elements have *too many* lines in the spectrum. Due to the crowding this causes at low resolution, almost any 20-Å swath of spectrum contains several lines of each of these elements. Finding good indices is a matter of choosing lesser evils. Our candidates are Fe4058, Fe4930, Ni3667, Ni3780, Ni4292, Ni4910, Ni4976, Ni5592, Cr3594, Cr4264, Cr5206, Mn3794, Mn4018, Mn4061, and Mn4757. Cr3594 is illustrated in Figure 6 and Ni4976 is illustrated in Figure 7. These choices partly arise from the increased volatility in the blue portions of the spectrum which amplifies the relative spectral response. The bottom line is that the abundances of all of these elements should be fairly easy to measure, but most indices meant to measure *other* elements will be stuck with some contribution from these four.

3.6. Sc, Ti, V

We illustrate examples of spectral responses for Sc, Ti, and V in Figures 8, 9, and 10, respectively. Indices V4112, V4928, V6604, Sc3613, Sc4312, and Sc6292 each yield detections between 1-σ and 2-σ, so measurement of all of them should yield $> 2\sigma$ abundances for V and Sc. The Ti indices Ti4296, Ti4533, and Ti5000 cluster around 2.5σ. Worthey (1998) raised

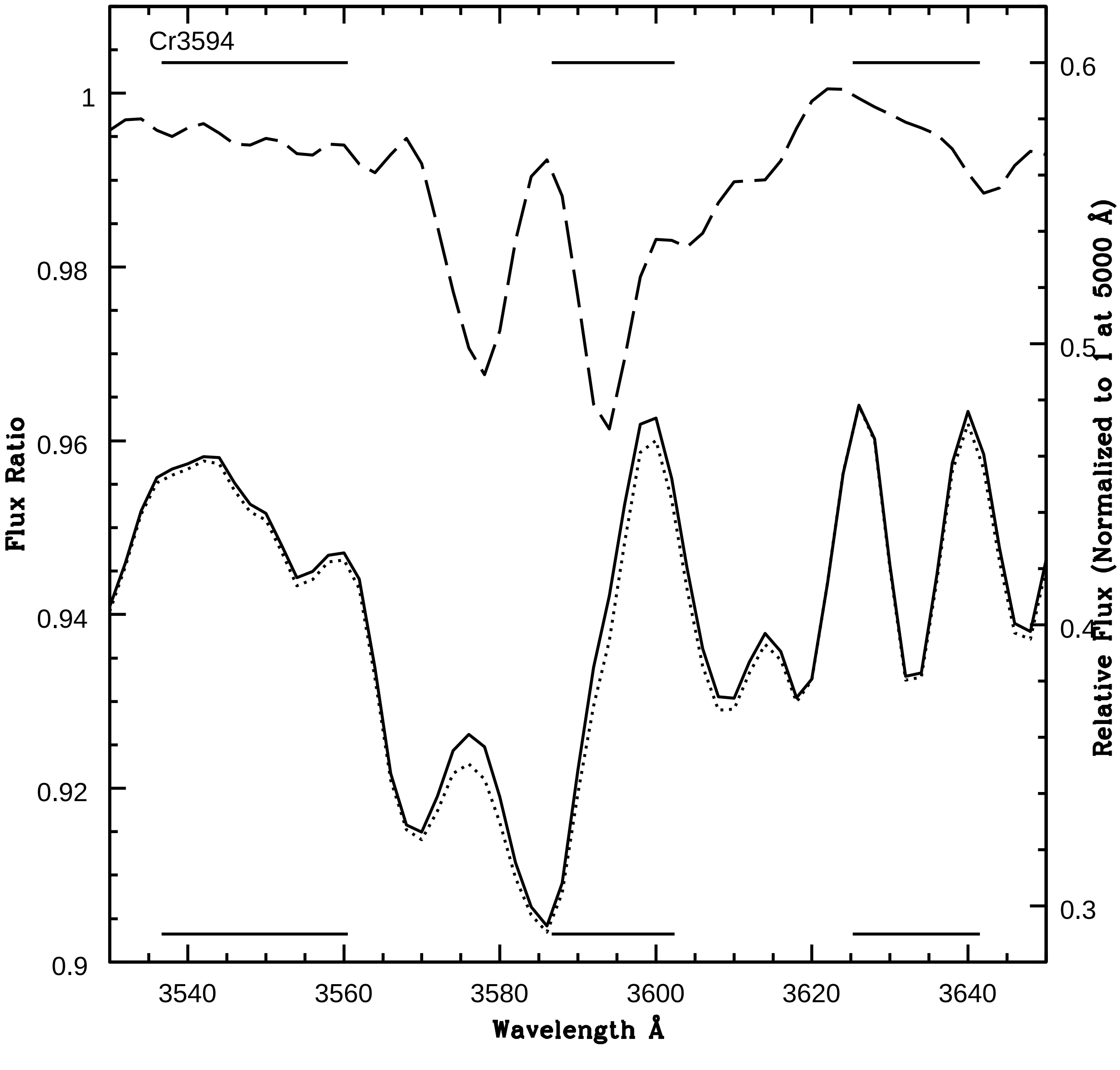

Fig. 6.— The Cr3594 index (*horizontal lines*). The Cr-enhanced (*dotted*) and normal (*solid*) spectra are overplotted near the bottom with scale to the right. The ratio of the two spectra are shown (*dashed*) at the top, with scale to the left.

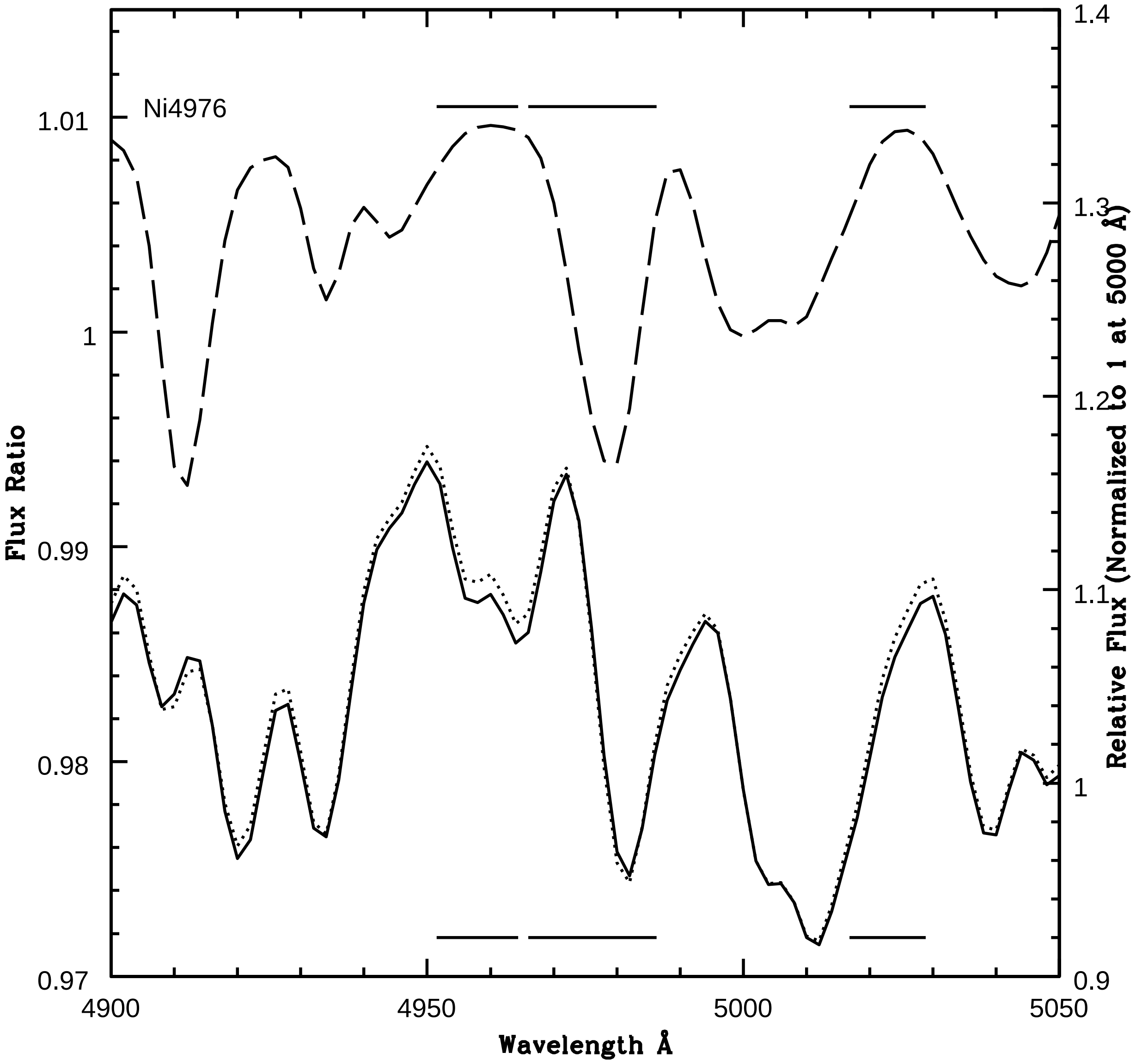

Fig. 7.— The Ni4976 index (*horizontal lines*). The Ni-enhanced (*dotted*) and normal (*solid*) spectra are overplotted near the bottom with scale to the right. The ratio of the two spectra are shown (*dashed*) at the top, with scale to the left.

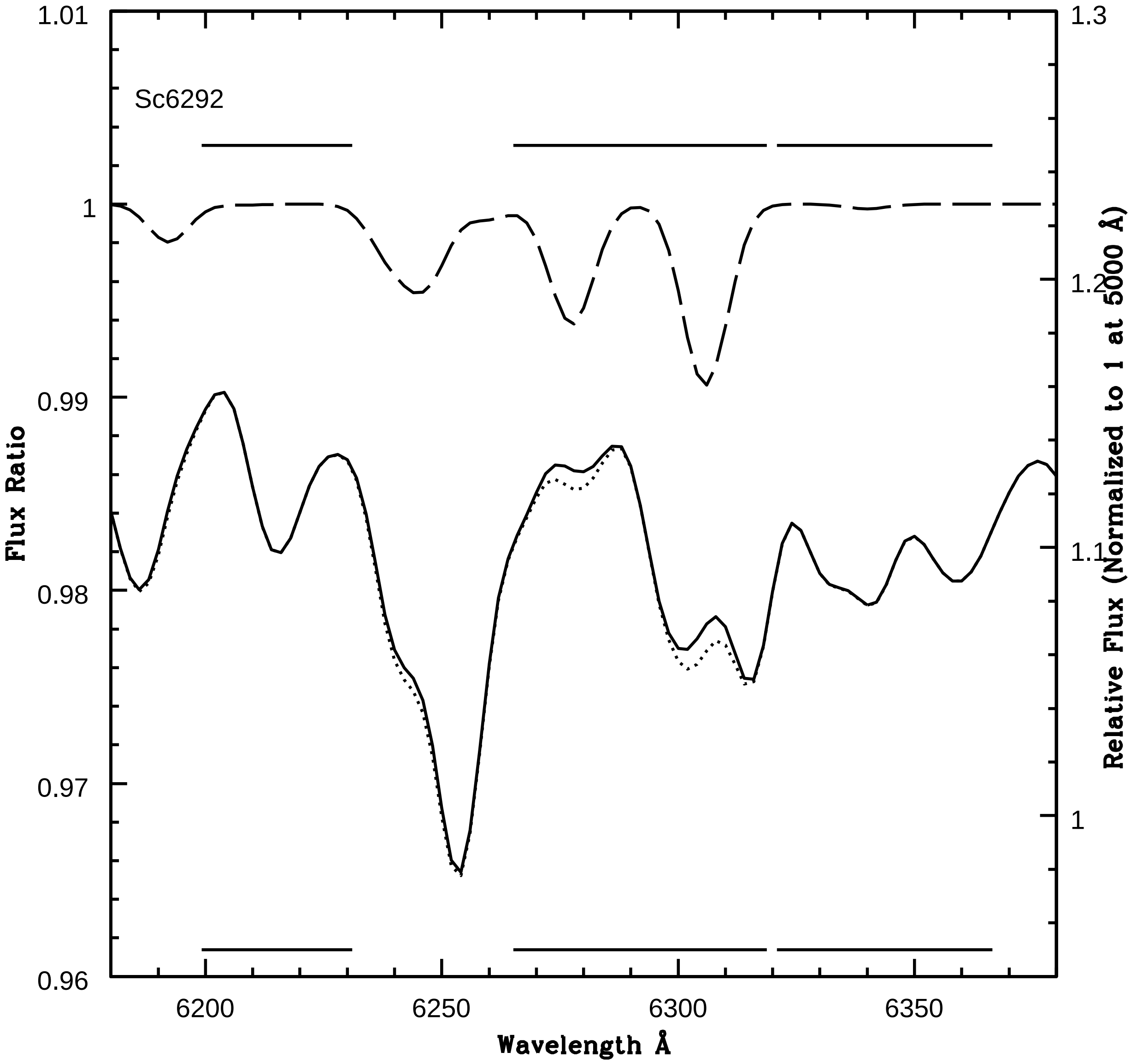

Fig. 8.— The Sc6292 index (*horizontal lines*). The Sc-enhanced (*dotted*) and normal (*solid*) spectra are overplotted near the bottom with scale to the right. The ratio of the two spectra are shown (*dashed*) at the top, with scale to the left.

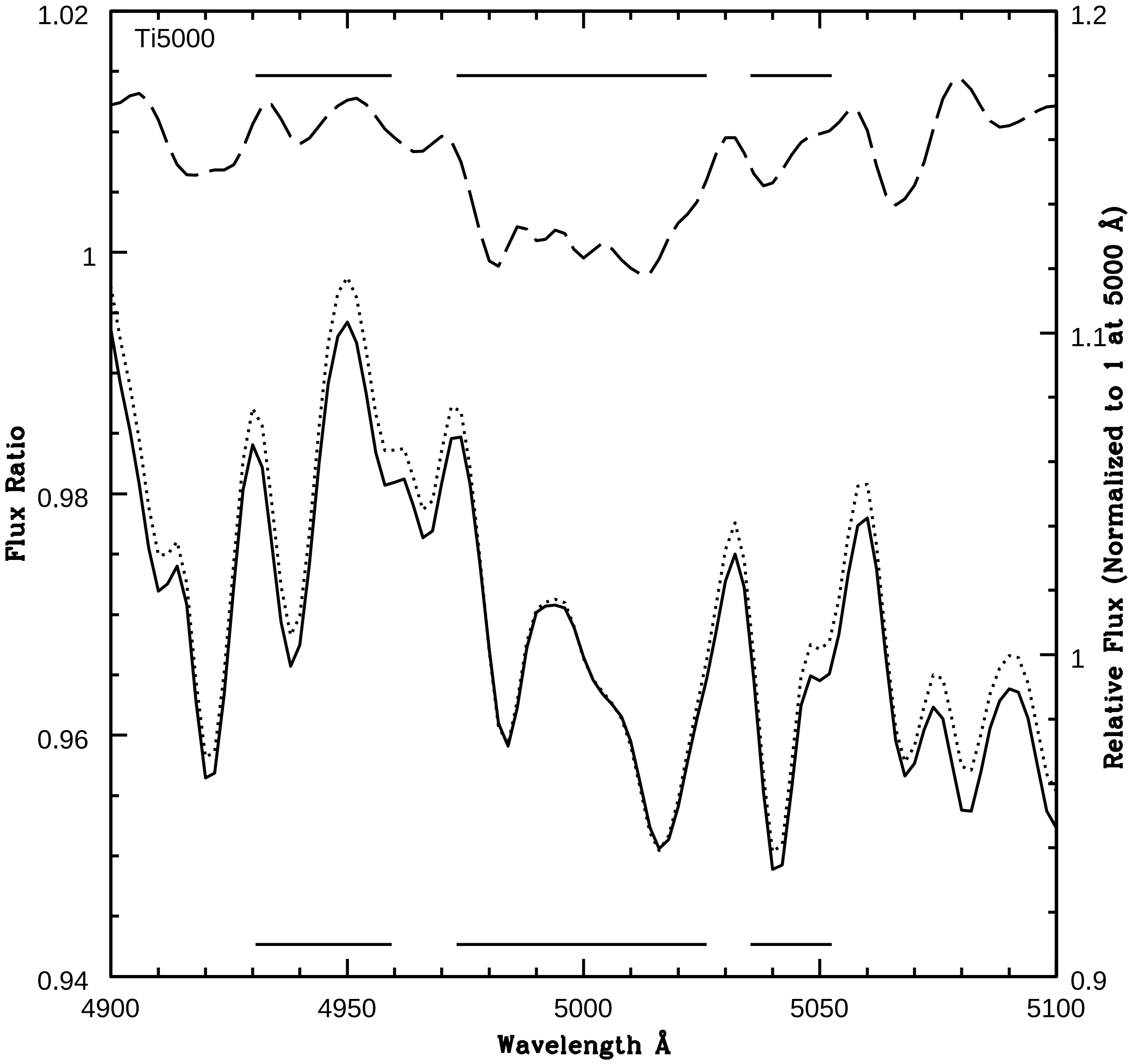

Fig. 9.— The Ti5000 index (*horizontal lines*). The Ti-enhanced (*dotted*) and normal (*solid*) spectra are overplotted near the bottom with scale to the right. The ratio of the two spectra are shown (*dashed*) at the top, with scale to the left.

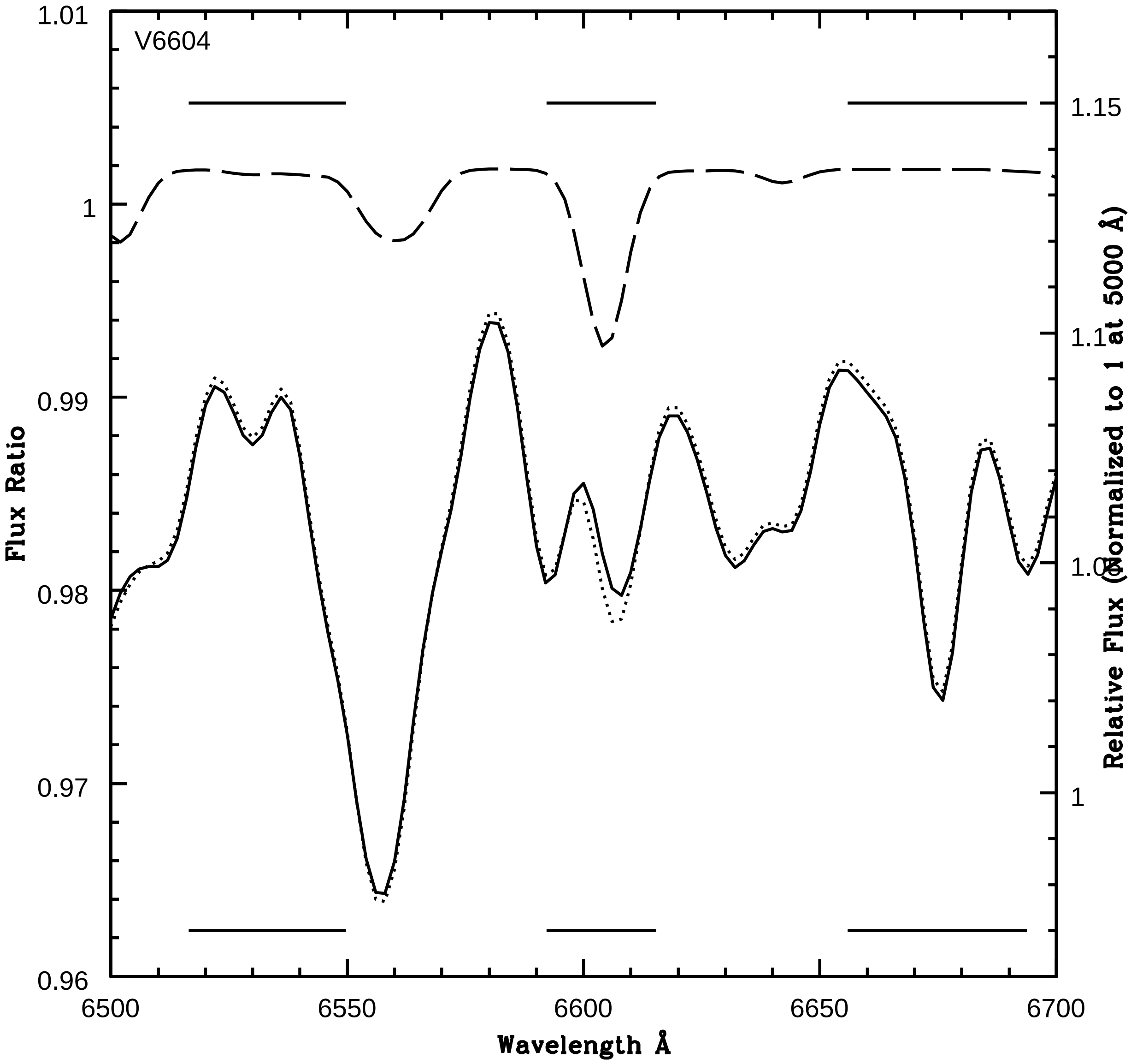

Fig. 10.— The V6604 index (*horizontal lines*). The V-enhanced (*dotted*) and normal (*solid*) spectra are overplotted near the bottom with scale to the right. The ratio of the two spectra are shown (*dashed*) at the top, with scale to the left.

issues of possible Ti-V-Sc interplay that should be resolved using these or similar indices.

3.7. Co, Cu, Zn

Heavier metals Co, Cu, and Zn are interesting from a nucleosynthetic standpoint since they lie beyond the iron peak. The best Co index is illustrated in Figure 11. There should be no problem measuring Co in real galaxies. Copper and zinc, on the other hand, are decidedly borderline at S/N = 100.

The Zn4720 index measures about a 1-σ spectral response, but many other elements produce a similar or greater spectral response. Index Cu5217 has effects due to C, Mg, and Cr that are much larger than the response due to Cu. Cu5780 has an even weaker response and Cr modifies the same spectral region. Zinc and Cu measurements may be possible, but will be difficult compared to most other elements we explore.

3.8. Sr, Ba, Eu

Abundances of Sr and Ba trace S-process enrichment, while Eu is thought to come mostly from R-process enrichment, and nucleosynthetic theory offers clear predictions for these elements. We find that Sr can be measured, but, like Al, only on one place in the spectrum. This is around the Sr II line at λ4077.71, with index Sr4076 (Figure 12). The result is favorable, with about a 4σ detection. In the cases of single lines being studied, as for Sr or Al, a lower velocity dispersion will result in much easier measurement (and a higher velocity dispersion in a much harder measurement).

Barium, on the other hand, is our most perfect element in the sense of having strong lines well separated from others and easily bracketed by index continua. All three indices, Ba4552, Ba4933 (Figure 13), and Ba6142, are fairly independent of other element ratios. The spectral responses are between 2σ and 4σ for all three definitions.

Europium has weaker lines than Ba, and the strongest one, measured by Eu3970, is tangled up with Ca, CN, and Si. The Eu4592 index (Figure 14) is tangled up with Ti, V, and Fe. And both are weak, only 0.5σ detections at S/N = 100. Europium can be measured, but it will take significant work to pull a reliable measurement from a real elliptical galaxy.

3.9. Abundance Effects on Colors and Other Established Index Systems

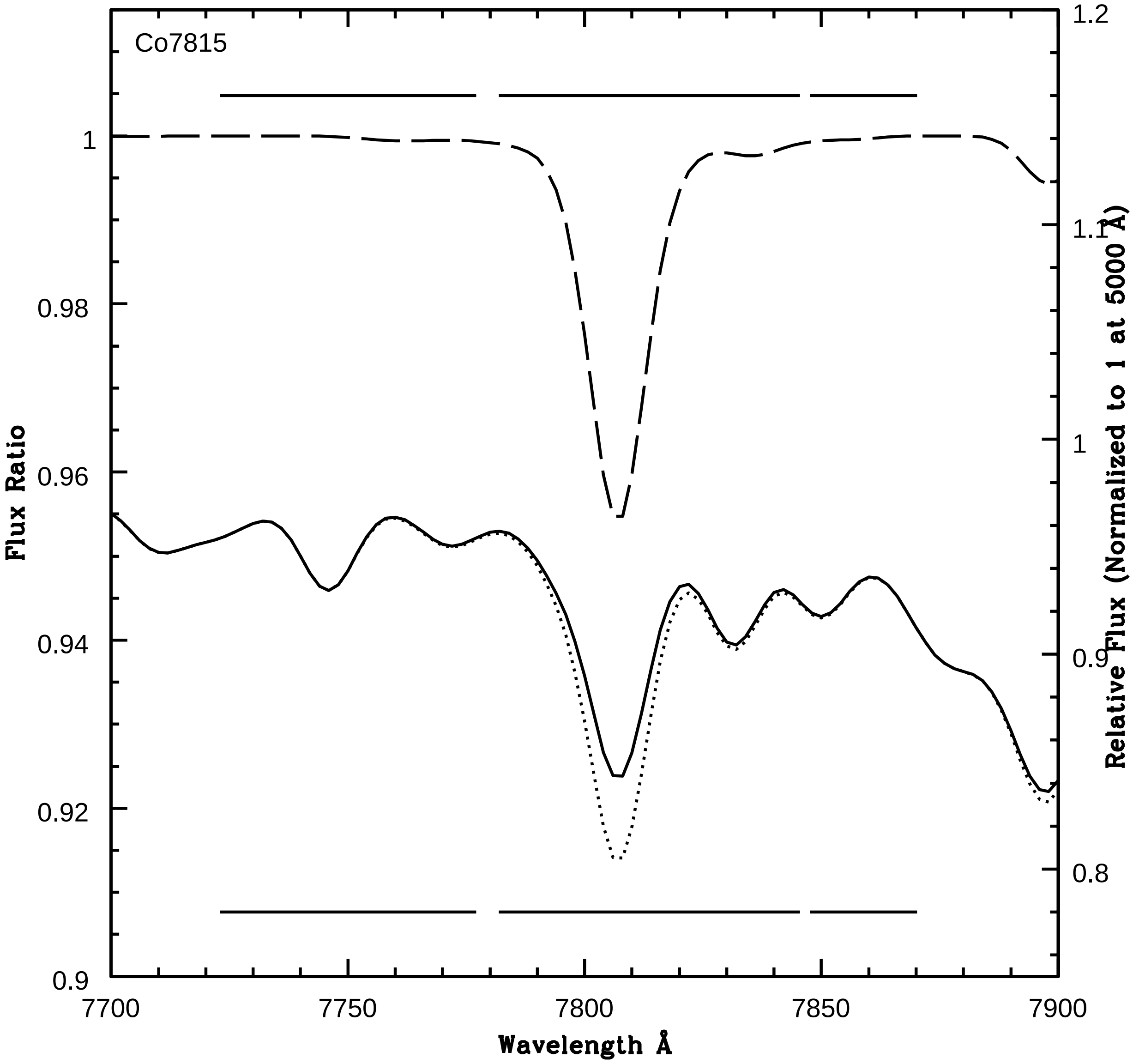

Fig. 11.— The Co7815 index definition (*horizontal lines*). The Co-enhanced (*dotted*) and normal (*solid*) spectra are overplotted near the bottom with scale to the right. The ratio of the two spectra are shown (*dashed*) at the top, with scale to the left.

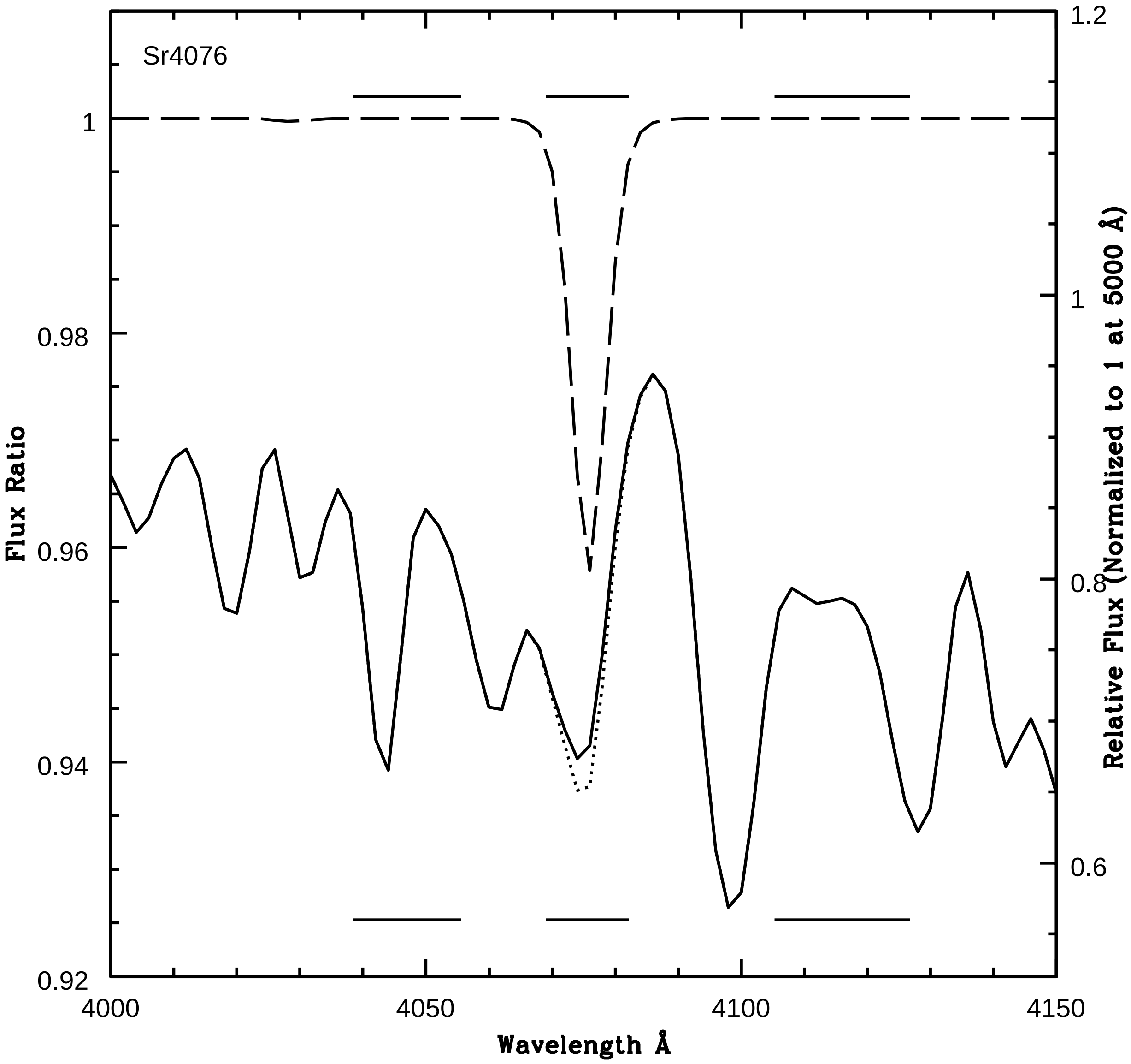

Fig. 12.— The Sr4076 index (*horizontal lines*). The Sr-enhanced (*dotted*) and normal (*solid*) spectra are overplotted near the bottom with scale to the right. The ratio of the two spectra are shown (*dashed*) at the top, with scale to the left.

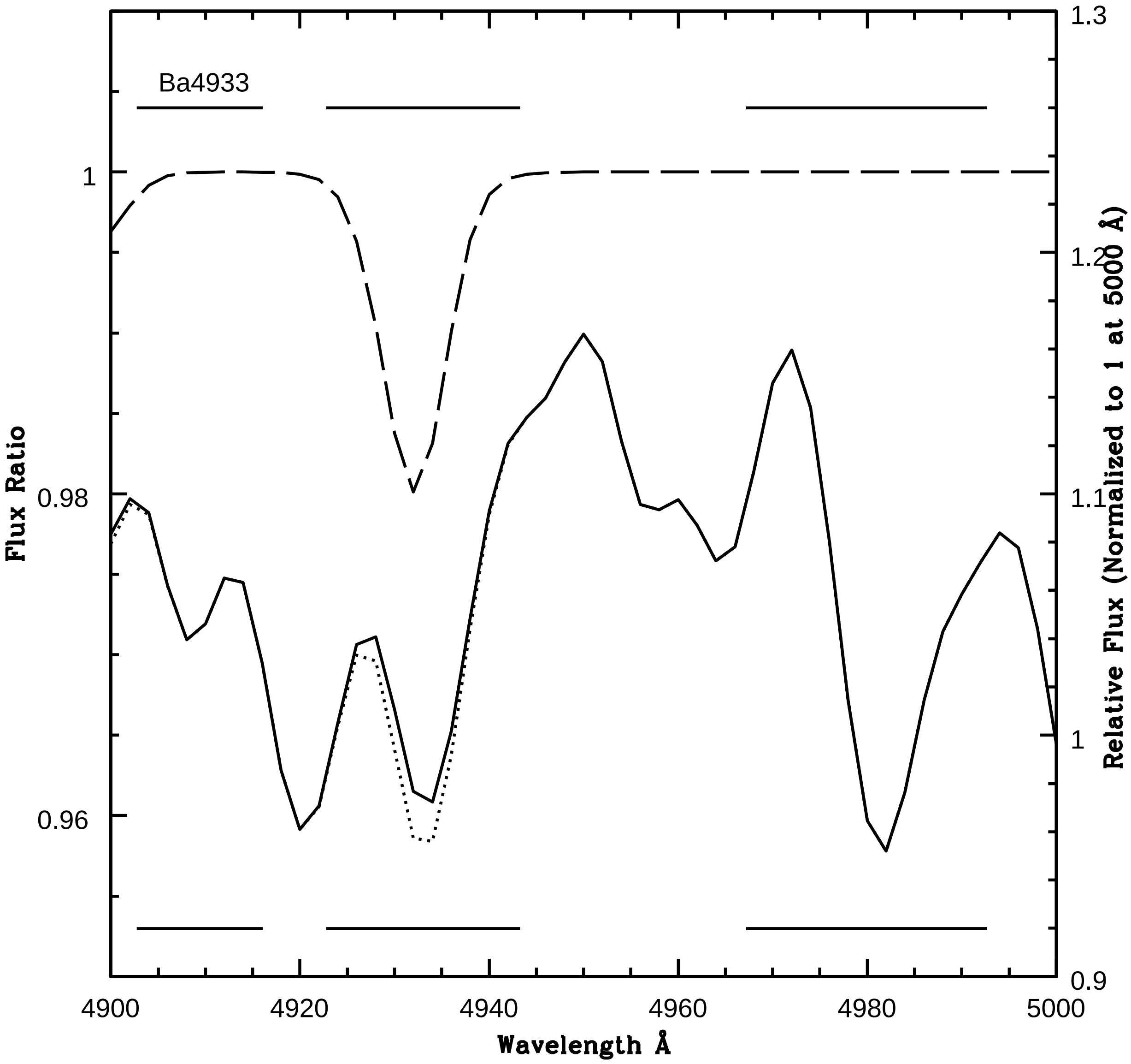

Fig. 13.— The Ba4933 index (*horizontal lines*). The Ba-enhanced (*dotted*) and normal (*solid*) spectra are overplotted near the bottom with scale to the right. The ratio of the two spectra are shown (*dashed*) at the top, with scale to the left.

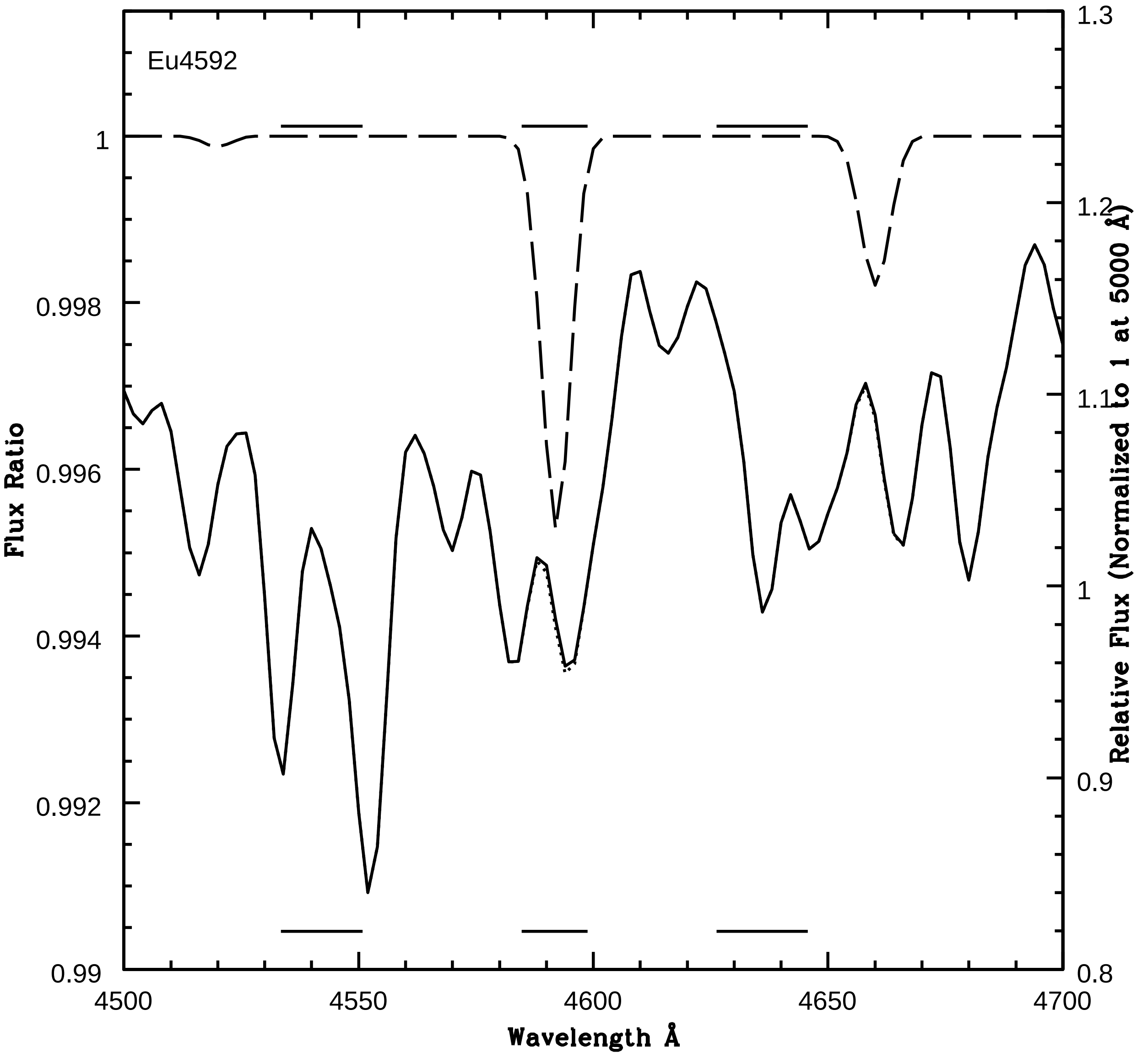

Fig. 14.— The Eu4592 index (*horizontal lines*). The Eu-enhanced (*dotted*) and normal (*solid*) spectra are overplotted near the bottom with scale to the right. The ratio of the two spectra are shown (*dashed*) at the top, with scale to the left.

Table 3. Spectral Responses to Element Enhancements for Established Index Systems

Name	I_O (Å)	σ (Å)	C	N	O	Na	Mg	Al	Si	S	K	Ca	Sc	Ti	V	Cr	Mn	Fe	Co	Ni	Cu	Zn	Sr	Ba	Eu	×2
CN_1	0.062	0.004	6.50	6.00	-4.75	-0.25	-0.50	0.00	0.25	0.00	0.00	-0.75	0.00	0.75	-1.00	-1.00	-0.25	-1.25	-0.25	0.00	0.00	0.00	0.25	0.50	0.00	2.75
CN_2	0.110	0.005	6.80	5.20	-4.20	-0.40	-1.00	0.00	1.00	0.00	0.00	-1.20	0.00	0.60	-0.60	-1.20	-0.40	-1.80	-0.20	0.00	0.00	0.00	0.20	0.20	0.00	3.00
Ca4227	1.756	0.067	-1.78	-1.78	3.03	-0.12	0.79	0.00	-0.24	0.00	0.00	7.21	-0.13	0.36	0.19	-0.36	-0.01	1.64	0.15	-0.06	0.00	0.00	-0.25	0.00	0.00	4.52
G4300	6.004	0.122	9.08	0.17	-1.78	-0.53	-1.16	-0.01	-1.33	0.01	0.00	0.79	0.77	2.16	0.11	-1.57	-0.06	-3.46	0.03	0.97	0.00	0.00	0.01	0.01	0.00	0.48
Fe4383	2.611	0.188	3.46	-0.04	-0.44	-0.07	-0.80	-0.02	-0.95	-0.01	0.00	-0.62	0.23	0.81	0.93	0.00	-0.29	2.43	0.00	-0.62	0.00	0.00	0.00	0.01	0.00	2.15
Ca4455	-0.112	0.103	2.33	-0.15	0.13	-0.01	0.00	0.01	-0.12	0.00	0.00	0.20	0.00	0.68	1.35	1.25	0.78	-1.20	0.07	-0.18	0.00	0.00	0.00	-0.01	0.00	1.99
Fe4531	3.226	0.151	3.11	0.03	0.11	0.15	-0.09	-0.01	-0.83	-0.01	0.00	-0.02	-0.22	2.36	0.38	0.97	-0.11	0.37	0.16	0.03	0.00	0.00	0.00	1.23	0.01	3.54
$C_2$4668	1.513	0.245	9.38	0.11	-3.54	-0.37	-0.76	0.00	-1.82	0.17	0.00	-0.05	-0.13	0.99	0.02	-0.78	-0.69	-0.10	-0.54	0.09	0.00	0.28	-0.06	-0.18	0.05	4.60
Hβ	3.260	0.093	0.76	0.03	0.15	0.04	-0.85	-0.02	-0.05	0.01	0.00	-0.05	-0.14	0.56	-0.18	-0.82	-0.08	-0.47	0.15	1.29	0.00	0.00	-0.18	-0.01	0.00	-0.34
Fe5015	5.264	0.217	2.99	0.06	0.27	0.14	-1.46	-0.02	-0.12	0.00	0.00	0.32	-0.50	1.93	0.06	0.23	-0.16	2.03	0.00	0.88	0.00	0.00	-0.11	0.00	0.00	4.12
Mg_1	0.051	0.002	15.50	0.50	-5.50	-1.50	14.50	0.00	-2.50	0.00	0.00	-1.50	0.00	0.50	0.00	-1.00	0.50	-7.00	0.00	1.00	0.50	0.00	0.00	-0.50	0.00	10.00
Mg_2	0.152	0.003	6.00	0.33	-0.33	-1.00	14.33	0.00	-1.33	0.00	0.00	-0.67	-0.33	2.00	0.33	-0.67	0.00	-5.00	0.00	0.33	0.00	0.00	0.33	0.00	0.00	9.67
Mg b	1.714	0.114	-0.46	0.05	0.89	-0.54	7.24	-0.04	-0.40	-0.01	0.00	-0.14	-0.01	0.27	0.11	-1.54	-0.01	-2.10	0.16	-0.30	-0.01	0.00	-0.04	-0.09	-0.01	2.18
Fe5270	3.486	0.118	2.03	0.12	-0.07	-0.12	-0.59	-0.03	-0.19	0.03	0.00	0.80	-0.32	0.18	-0.27	0.38	0.00	1.71	0.19	0.18	-0.01	0.00	-0.01	0.00	0.00	2.77
Fe5335	4.325	0.130	2.28	0.03	0.09	-0.15	-0.55	-0.03	-0.22	-0.01	0.00	-0.20	0.27	0.31	0.02	0.95	0.08	3.83	0.24	0.11	0.00	0.00	0.01	0.00	-0.01	4.75
Fe5406	1.266	0.105	0.84	0.05	0.04	-0.10	-0.37	0.00	-0.21	0.00	0.00	-0.10	0.18	0.28	0.30	0.45	-0.04	2.23	-0.04	-0.03	0.00	0.00	0.00	-0.02	0.00	2.43
Fe5709	1.527	0.082	1.56	0.00	-0.11	-0.33	0.12	-0.02	-0.01	0.00	0.00	0.09	-0.02	0.65	-0.29	0.18	-0.06	1.44	0.00	0.10	0.21	0.00	0.00	-0.05	0.00	2.95
Fe5782	0.344	0.083	0.76	0.04	-0.10	-0.02	0.14	-0.01	0.01	0.00	0.00	-0.17	0.00	-0.27	0.12	2.13	0.04	-0.14	0.00	0.34	0.41	0.00	0.00	-0.07	0.00	2.46
Na D	4.291	0.099	1.81	0.15	0.14	8.96	-0.35	-0.02	-0.35	0.00	0.00	-0.11	0.00	0.17	0.03	-0.03	0.00	0.25	0.00	-0.06	0.00	0.00	0.00	0.05	0.00	8.08
TiO_1	-0.005	0.002	0.50	0.50	1.50	0.00	0.00	0.00	0.00	0.00	0.00	0.00	0.50	2.00	-0.50	0.50	0.00	0.00	0.50	0.00	0.00	0.00	0.00	0.00	0.50	2.00
TiO_2	0.008	0.002	0.50	0.00	5.50	0.00	-0.50	0.50	-0.50	0.00	0.00	-0.50	1.00	3.00	1.00	0.50	0.00	1.00	0.00	0.00	0.00	0.00	0.00	-0.50	0.00	5.50
Hδ_A	-1.541	0.136	-3.03	0.00	0.15	0.10	0.21	0.00	1.83	0.01	-0.07	0.55	-0.37	-1.30	2.06	0.06	-0.64	-5.22	0.06	0.10	0.00	0.00	-1.13	-0.04	0.00	-2.99
Hγ_A	-4.699	0.144	-7.01	-0.26	0.65	0.48	1.69	0.03	1.54	0.01	0.00	-0.41	-0.75	-2.26	-0.96	0.69	-0.07	-0.18	-0.02	-0.44	-0.01	0.00	-0.01	0.08	0.00	-2.60
Hδ_F	1.294	0.089	-2.39	0.31	-0.45	-0.09	-0.34	-0.01	2.18	0.01	0.00	0.66	-0.02	-1.22	1.90	-0.58	-0.43	-3.18	-0.16	-0.17	0.00	0.00	-0.92	-0.02	-0.04	-1.25
Hγ_F	-0.560	0.088	-3.35	-0.14	0.95	0.37	1.06	0.01	1.43	0.01	0.00	-0.39	-0.36	-0.47	-0.42	0.33	0.01	-0.11	-0.01	-0.78	0.00	0.00	0.00	0.14	0.00	-1.10
Hα	1.248	0.091	0.09	0.25	-0.64	0.04	-0.11	-0.03	0.25	0.00	0.00	-0.09	-0.01	-0.01	0.07	-0.14	0.00	-0.96	-0.15	-0.11	0.00	0.00	0.01	-0.01	-0.03	-0.45
Hδ/4045	0.855	0.012	-1.18	-0.95	0.51	0.10	0.29	0.01	-2.17	-0.01	0.28	0.14	0.41	0.17	-1.06	-0.22	0.05	4.04	0.00	0.03	0.00	0.00	0.00	0.00	0.00	0.66
Hδ/4063	0.803	0.011	-0.02	-0.73	0.36	0.11	0.35	0.01	-2.25	-0.01	0.00	-0.04	-0.02	0.72	-0.99	-0.19	0.69	3.66	0.03	0.07	0.00	0.00	0.00	0.00	0.00	0.62
Sr II/4045	1.012	0.012	-2.39	-0.46	0.07	-0.02	-0.09	0.00	-0.01	0.00	0.32	0.23	0.48	-0.55	0.06	0.01	-0.04	4.25	-0.27	0.00	0.00	0.00	-2.83	0.00	0.00	-0.03
Sr II/4063	0.951	0.012	-0.99	-0.19	-0.11	-0.01	-0.02	0.00	-0.13	0.00	0.00	0.02	-0.01	0.13	0.07	0.04	0.69	3.79	-0.22	0.04	0.00	0.00	-2.66	0.00	0.00	-0.06
Hγ/4325	1.010	0.013	0.93	0.03	-0.33	-0.10	-0.38	-0.02	-0.28	-0.01	0.00	-0.06	0.03	-0.17	0.30	-0.66	-0.02	2.53	0.00	0.14	0.00	0.00	0.00	0.00	0.00	1.34
4289/4271	0.943	0.012	-1.78	0.02	-0.03	0.25	-0.15	-0.01	-0.16	0.00	0.00	-0.74	-0.02	-0.87	-0.21	1.37	0.02	1.76	-0.03	-0.90	0.00	0.00	0.00	0.00	0.00	1.00
4384/4352	0.938	0.013	0.16	-0.05	-0.05	0.09	0.92	0.00	0.55	0.00	0.00	0.13	0.01	-0.09	-0.07	0.23	-0.03	-1.52	0.00	-0.02	0.00	0.00	0.00	0.10	0.00	-0.65
Ca II	1.279	0.007	1.37	0.01	0.21	-0.13	-0.74	-1.73	-1.95	-0.03	0.00	9.21	0.00	-0.14	0.70	-0.45	0.01	-2.42	0.26	-0.58	0.00	0.00	0.00	0.01	-1.05	3.35
H8/3859	0.908	0.010	3.08	6.21	-1.00	0.02	0.80	0.01	-0.64	-0.02	0.00	-0.85	0.00	0.09	0.29	0.54	0.00	-2.34	-0.33	0.32	0.00	0.00	0.00	-0.12	0.00	4.37
3550/3544	1.000	0.009	1.02	0.04	-0.22	0.00	0.24	0.00	-0.11	0.00	0.00	-0.04	0.00	-0.34	0.00	-0.06	0.00	-0.19	0.00	0.00	0.00	0.00	0.00	0.00	0.00	-0.64
Hn/Fe	0.925	0.007	1.43	2.55	-0.41	0.01	0.33	0.00	-1.77	-0.02	0.16	-0.38	0.26	0.03	-0.29	-0.28	0.02	2.82	-0.16	0.27	0.00	0.00	0.00	-0.06	0.00	3.41

The first 21 absorption feature indices listed in Table 3 are from Worthey et al. (1994), then 4 Balmer indices from Worthey & Ottaviani (1997), and the Hα index from Cohen et al. (1998). These are all equivalent widths [although CN_1, CN_2, Mg_1, Mg_2, TiO_1, and TiO_2 are expressed in magnitudes (Worthey et al. 1994)] with two bandpasses defining a pseudocontimuum and a central bandpass over which the pseudocontinuum-flux difference is integrated. The next 10 indices in Table 3 are from Rose (1994) and the final index is the Hn/Fe average index (Hn/Fe = $\langle$Hγ/λ4325 + Hδ/λ4045 + H8$/\lambda$3859 $\rangle$) from Caldwell & Rose (1998). These are line-depth ratios defined by dividing the fluxes at the centers of absorption features. As such they are more sensitive to velocity dispersion than the equivalent-width style of index. For the error estimate in the ratio indices we assumed a 2-Å bandpass for calculating S/N. In many of our spectra it was impossible to centroid correctly for the components of the 3550/3544 index because these particular features do not appear distinctly enough in the broadened synthetic spectra. We adopted the flux point closest to the index wavelength and computed responses anyway, but the 3550/3544 result should be considered even more approximate than the rest of these exploratory and approximate results.

The results in Table 3 roughly agree with previously published integrated-light models (Thomas et al. 2004; Trager et al. 2000a,b) in the sign and order of magnitude of the response, but it is difficult to be more quantitative given the sketchiness of our two-star "galaxy". At the stellar level, we can compare Tripicco & Bell (1995) with HTWB (2002). For the giant star (T_{eff} = 4255, log g = 1.90) the responses always agree to better than a factor of two, and usually to about 10%, with three exceptions: (1) responses less than a few tenths of a σ because of roundoff, etc., (2) the quadratic carbon effect in indices affected by C abundance because we avoid the nonlinear regime, and (3) the two TiO indices because Tripicco & Bell (1995) did not have TiO line lists.

The differential effects of abundance on Johnson/Cousins $BRVI$ colors are given in Table 4. The second column is the color of the "galaxy" and the remaining columns are the abundance responses in units of millimagnitudes. The colors were calculated as in Worthey (1994). The effects are mild, the largest one being that of carbon, where a 0.15 dex increase in C abundance reddens $B-V$ by 0.04 mag. $B-V$ suffers more than any other color from abundance effects (U band is probably even worse, but our spectra did not reach quite blue enough to measure U).

4. Discussion, Summary, and Conclusion

Of 23 elements explored, 18 look favorable for measurement in S/N $>$ 100 integrated spectra of star clusters, elliptical galaxies, S0 galaxies, spiral galaxy bulges, and some parts of spiral galaxy disks. These results hold true even in galaxies of high velocity dispersion. The the situation becomes more favorable for systems with low velocity dispersion. The 5 unfavorable elements are not impossible to measure, but given the small amount of spectral change that results from abundance changes, along with confusion from other elements, S, K, Cu, Zn, and Eu will be more challenging. The precision of abundance ratio measurements can be expected to reach 0.01 dex in favorable cases [see Worthey (2004)], although the real accuracy of measurement is model-dependent at the moment. The 18 favorable elements can be measured with precision $<$ 0.1 dex, except V, which is borderline.

Table 2 and Table 3 plus equations 4 and 5 give a more detailed look at expected precisions. For example, [Al/Fe] is measured to 4.5σ at S/N $=$ 100 using the Al3953 index, so its 1-σ precision would be 0.3 dex / $4.5\sigma \approx 0.07$ dex. S/N $=$ 200 spectra should yield $\approx$0.03 dex precision. Obviously, some caution should be exercised, as we assume perfect models and also assume that photon noise is the only error source. Ultimate accuracy (as opposed to observational precision) will depend on the quality of the models used to fit the integrated spectra. In this Al3953 example, the synthetic spectra will need to accurately reproduce all atomic and molecular lines in that spectral region, as well as treating the wings of the Ca H and K lines correctly, at least in a differential sense. Since empirical stellar spectra can and will be used to model the unadjusted integrated spectral models, the synthetic spectra will only be needed in a differential sense.

We also tabulate abundance responses for Lick/IDS indices, Rose indices, and $BVRI$ colors to assess the opportunities (or vulnerabilities) for measuring abundance ratio effects (or being insensitive to them). For instance, the 0.04 mag change in $B-V$ caused by a 0.15 dex enhancement of carbon is the same as the color change in bright cluster galaxies over a 1-magnitude range of brightness along the color-magnitude relation (Lugger 1984). Since we suspect that the spectral changes in large elliptical galaxies may be mostly due to elements lighter than the Fe group (Trager et al. 2000b) this indicates that, even if the addition of light elements does *not* cause the giant branch to become cooler, colors will become somewhat more red via the enhanced line blanketing.

This promising avenue of research (18 individual element abundance ratios with $0.01 \lesssim \sigma \lesssim 0.1$ from integrated stellar light) should open up new areas of investigations into the nucleosynthesis of external galaxies, especially early-type galaxies. There is no reason that very distant galaxies and extragalactic globular cluster systems could not be studied using the same techniques, except for the old problem of gathering enough photons for high quality spectra.

We would like to thank M. Houdashelt for providing the spectra associated with HTWB and Roger Bell for the use of the SSG program. Major funding was provided by National Science Foundation grant number 0307487, the New Standard Stellar Population Model (NSSPM) project.

REFERENCES

Bell, R. A., Paltoglou, G., & Tripicco, M. J. 1994, MNRAS, 268, 771

Bruzual, G., & Charlot, S. 2003, MNRAS, 344, 1000

Buzzoni, A. 1989, ApJS, 71, 817

Caldwell, N., & Rose, J. A. 1998, AJ, 115, 1423

Castelli, F., & Kurucz, R. L. 2004, A&A, 419, 725

Cohen, J. G., Blakeslee, J. P., & Ryzhov, A. 1998, ApJ, 496, 808

Gustafsson, B., Bell, R. A., Eriksson, K., & Nordlund, Å. 1975, A&A, 42, 407

Houdashelt, M. L., Trager, S. C., Worthey, G., & Bell, R. A. 2002, BAAS, 201, 14.05 (HTWB)

Jasckek, C., & Jaschek, M. 1995, The Behavior of Chemical Elements in Stars, (Cambridge University Press: Cambridge)

Knapp, G. R. 1999, in ASP Conf. Ser. 163, Star Formation in Early-Type Galaxies, ed. P. Carral & J. Cepa (San Francisco: ASP), 119

Kurucz, R. L. 1995, in Laboratory and Astronomical High Resolution Spectra, ASP Conf. Ser. 81, ed. A. J. Sauval, R. Blomme, & N. Grevesse (Astron. Soc. Pac.: San Francisco), 17

Lugger, P. M. 1984, ApJ, 278, 51

Maraston, C., Greggio, L., Renzini, A., Ortolani, S., Saglia, R. P., Puzia, T. H., Kissler-Patig, M. 2003, A&A, 400, 823

Maraston, C. 2005, MNRAS, submitted (astro-ph/0410207)

Meggers, W. F., Corliss, C. H., & Scribner, B. F. 1975, National Bureau of Standards Monograph 145, (U. S. Government Printing Office: Washington, D. C.)

Oosterloo, T. A., Morganti, R., Sadler, E., Vergani, D., & Caldwell, N. 2002, AJ, 123, 729

Proctor, R. N., & Sansom, A. E. 2002, MNRAS, 333, 517

Rose, J. A. 1994, AJ, 107, 206

Tantalo, R., & Chiosi, C. 2004, MNRAS, 353, 917

Thomas, D., Maraston, C., & Bender, R. 2003, MNRAS, 339, 897

Thomas, D., Maraston, C., & Korn, A. 2004, MNRAS, 351, L19

Tonry, J. T. 1985, AJ, 90, 2431

Trager, S. C., Faber, S., M., Worthey, G., & González, J. J. 2000, AJ, 119, 1645

Trager, S. C., Faber, S., M., Worthey, G., & González, J. J. 2000, AJ, 120, 165

Tripicco, M. J., & Bell, R. A. 1995, AJ, 110, 3035

Valdes, F., Gupta, R., Rose, J. A., Singh, H. P., & Bell, D. P. 2004, ApJS, 152, 251

Welty, D. E., Hobbs, L. M., & Kulkarni, V. P. 1994, ApJ, 436, 152

Worthey, G., Faber, S. M., & González, J. J. 1992, ApJ, 398, 69

Worthey, G., Faber, S. M., González, J. J., & Burstein, D. 1994, ApJS, 94, 687

Worthey, G., & Ottaviani, D. L. 1997, ApJS, 111, 377

Worthey, G. 1994, ApJ, 95, 107

Worthey, G. 1998, PASP, 110, 888

Worthey, G. 2004, AJ, 128, 2826

This preprint was prepared with the AAS LATEX macros v5.2.

Table 4. Color Responses to Element Enhancements in Millimagnitudes

Name	Color	C	N	O	Na	Mg	Al	Si	Ca	Ti	V	Cr	Mn	Fe	Ni	×2
								Dwarf								
$B-V$	0.491	25	2	0	0	-4	0	-2	5	3	1	3	0	12	0	26
$V-R_C$	0.283	7	0	0	0	0	0	0	0	0	0	1	0	6	0	5
$V-I_C$	0.576	7	0	0	0	-1	0	-1	-1	1	0	1	0	8	0	-1
R_C-I_C	0.293	0	0	0	0	0	0	0	-1	0	0	0	0	1	0	-6
								Giant								
$B-V$	1.263	52	7	-25	-5	-28	0	15	7	7	3	10	2	19	1	57
$V-R_C$	0.642	10	-5	0	-1	7	0	0	-1	3	0	4	0	13	1	19
$V-I_C$	1.224	2	-11	10	0	9	1	0	-3	5	1	5	0	19	1	15
R_C-I_C	0.582	-8	-6	10	0	1	0	0	-1	2	0	1	0	5	0	-4
								"Galaxy"								
$B-V$	0.861	37	3	-9	-2	-12	0	3	6	7	2	6	1	15	2	42
$V-R_C$	0.501	10	-3	0	-1	5	0	-1	0	3	0	3	0	11	1	16
$V-I_C$	0.989	5	-8	8	0	7	1	0	-2	7	1	4	0	16	2	13
R_C-I_C	0.488	-4	-5	7	0	2	0	0	-1	3	0	1	0	5	0	-2